Mon. Not. R. Astron. Soc. **390,** 1133–1156 (2008) doi:10.1111/j.1365-2966.2008.13828.x

The anisotropic distribution of satellite galaxies

Jeremy Bailin,[1,2⋆] Chris Power,[2,3⋆] Peder Norberg,[4,5⋆] Dennis Zaritsky[6⋆] and Brad K. Gibson[7⋆]

[1]*Department of Physics & Astronomy, McMaster University, 1280 Main Street W, Hamilton, ON, L8S 4M1, Canada*
[2]*Centre for Astrophysics and Supercomputing, Swinburne University of Technology, Mail H39, PO Box 218, Hawthorn, Victoria, 3122, Australia*
[3]*Theoretical Astrophysics Group, Department of Physics and Astronomy, University of Leicester, Leicester LE1 7RH*
[4]*The Scottish Universities Physics Alliance (SUPA), Institute for Astronomy, University of Edinburgh, Royal Observatory, Blackford Hill, Edinburgh EH9 3HJ*
[5]*ETHZ Institut für Astronomie, HPF G3.1, ETH Hönggerberg, CH-8093 Zürich, Switzerland*
[6]*Steward Observatory, University of Arizona, 933 North Cherry Avenue, Tucson, AZ 85721, USA*
[7]*Centre for Astrophysics, University of Central Lancashire, Preston PR1 2HE*

Accepted 2008 August 10. Received 2008 June 30; in original form 2007 June 8

ABSTRACT

We identify satellites of isolated galaxies in the Sloan Digital Sky Survey and examine their angular distribution. Using mock catalogues generated from cosmological *N*-body simulations, we demonstrate that the selection criteria used to select isolated galaxies and their satellites in large galaxy redshift surveys must be very strict in order to correctly identify systems in which the primary galaxy dominates its environment. We demonstrate that the criteria used in many previous studies instead select predominantly group members. We refine a set of selection criteria for which the group contamination is estimated to be less than 7 per cent and present a catalogue of the resulting sample.

The angular distribution of satellites about their host is biased towards the major axes for spheroidal galaxies and probably also for red disc galaxies (the 'intermediate' class of Bailin & Harris), but is isotropic for blue disc galaxies, i.e. it is the colour of the host that determines the distribution of its satellites rather than its morphology. The similar anisotropy measured in this study to studies that were dominated by groups implies that group-specific processes are not responsible for the angular distribution. Satellites that are most likely to have been recently accreted, late-type galaxies at large projected radii, show a tendency to lie along the same axis as the surrounding large-scale structure. The orientations of isolated early- and intermediate-type galaxies also align with the surrounding large-scale structures.

We discuss the origin of the anisotropic satellite distribution and consider the implications of our results, critically assessing the respective roles played by the orientation of the visible galaxy within its dark matter halo, anisotropic accretion of satellites from the larger scale environment, and the biased nature of satellites as tracers of the underlying dark matter subhalo population.

Key words: galaxies: clusters: general – galaxies: dwarf – galaxies: formation – galaxies: haloes – galaxies: structure – dark matter.

1 INTRODUCTION

The spatial distribution of satellites around isolated galaxies can provide important insights into the mass distribution in and around these galaxies. If dynamical effects could be neglected and we could assume that satellite galaxies inhabit an unbiased set of dark matter subhaloes, then we would expect satellites to cluster preferentially along the major axis of the host dark matter halo of the primary galaxy, as in galaxy cluster mass haloes (Knebe et al. 2004). We could therefore determine the orientation of the parent galaxy within its dark matter halo by using the spatial distribution of its satellite galaxies.

However, there is good reason to believe that dynamical effects will play an important role in determining the spatial distribution of satellites. For example, Hartwick (2000) has argued that the imprint of anisotropic infall of satellites along filaments is evident

⋆E-mail: bailinj@mcmaster.ca (JB); cbp1@le.ac.uk (CP); iprn@roe.ac.uk (PN); dzaritsky@as.arizona.edu (DZ); bkgibson@uclan.ac.uk (BKG)

in the orbits of recently accreted systems, and Peñarrubia, Kroupa & Boily (2002) have shown that the inclination of a satellite's orbit can determine its dynamical response to the disc or spheroid of its parent galaxy. There is also a good reason to suspect that the relationship between satellites and the underlying dark matter subhalo population may not be straightforward, as has been argued by, for example, Gao et al. (2004) (but see Conroy, Wechsler & Kravtsov 2006). Indeed, current galaxy-formation models indicate that satellite galaxies represent a biased subset of subhaloes whose spatial distribution is very likely to be anisotropic within their parent galaxy's dark matter halo (e.g. Libeskind et al. 2005; Zentner et al. 2005), although current high-resolution models suggest that the orientation of the satellite system with respect to the dark matter halo is robust (Libeskind et al. 2007).

These considerations suggest that interpretation of the spatial distribution of satellites may be more complex than we might naïvely expect. Yet, despite these complexities, satellite galaxies represent a powerful observational probe into the mass distribution around galaxies. Therefore, it is essential to determine robustly the spatial distribution of satellite galaxies, and to establish whether or not they show a preferential alignment relative to their parent galaxies. This is the aim of the current study.

Locally, we see strong evidence for the preferential alignment or *anisotropic distribution* of satellites relative to their primary galaxies. Both the Milky Way and M31 have satellite populations that lie in great planes that are highly inclined to their discs. This has been noted by Lynden-Bell (1976), Hartwick (2000) and Kroupa, Theis & Boily (2005) for the Milky Way, by Koch & Grebel (2006) and McConnachie & Irwin (2006) for subsamples of satellites of M31 and by Metz, Kroupa & Jerjen (2007), who performed an analysis of the statistical significance of the planar distribution around both galaxies. The Milky Way and M31 are the only galaxies for which the sample of satellites is large enough that their spatial distribution is analysed directly (without requiring stacking to obtain a statistical sample). They are also the only systems for which we are certain that the satellites are physically associated with their primaries, and for which the three-dimensional positions of the satellites with respect to their primaries are known. In addition, proper motion measurements exist for a number of Milky Way satellites, which confirm that these systems are on polar orbits (Palma, Majewski & Johnston 2002).

Analysing the spatial distribution of satellites in external systems is generally more challenging because no more than one or two satellites are detected per primary galaxy, and because the three-dimensional location of the satellite with respect to its primary is uncertain. This measurement requires that primaries and their satellites be stacked to obtain statistical samples from which the projected angular distribution of satellites about a 'typical' primary is determined. Such an analysis was first performed by Holmberg (1969) for 58 isolated spiral and lenticular, or *late-type*, galaxies and their 218 optical companions, of which 75 were expected to be physically associated. He found that satellites at projected radii less than 50 kpc were more often found near the poles (minor axis) of the primary's disc (Fig. 1). This preferential polar distribution, referred to as the 'Holmberg Effect', was subsequently confirmed by Zaritsky et al. (1997b) (hereafter ZSFW) at larger projected radii of 300–500 kpc using a sample of 115 spectroscopically confirmed satellite galaxies of 69 isolated late-types.

The advent of large galaxy redshift surveys such as the 2dF Galaxy Redshift Survey (2dFGRS; Colless et al. 2001) and the Sloan Digital Sky Survey (SDSS; York et al. 2000) has enabled this issue to be revisited. These surveys provide an abundance

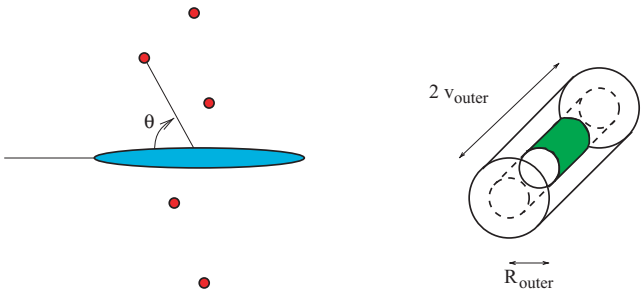

Figure 1. Left-hand panel: according to the Holmberg Effect, satellites of disc galaxies tend to lie near the minor axis of the disc. This corresponds to an angle between the major axis of the galaxy and the satellite (the 'disc angle', θ) of greater than 45°. Right-hand panel: selection cylinders around a potential primary galaxy, which lies at the centre of the cylinders. The outer isolation cylinder is marked with solid lines and has radius $R_{\rm outer}$ and length $2v_{\rm outer}$. The inner isolation cylinder is marked with dashed lines and has radius $R_{\rm inner}$ and length $2v_{\rm inner}$. The satellites are drawn from the shaded cylinder with radius $R_{\rm sat}$ and length $2v_{\rm sat}$.

of galaxies with spectroscopic redshifts, and several recent studies have sought to use numbers of galaxies far in excess of those that were available to Holmberg (1969) and ZSFW to address the question of spatial anisotropy with *significantly improved statistics*. Sales & Lambas (2004) (hereafter SL04) used over 2000 satellites of almost 1500 primary galaxies in the 2dFGRS, and found that satellites around blue primaries tended to follow an isotropic distribution, whereas the locations of low-velocity ($|\Delta v| < 160\,{\rm km\,s^{-1}}$) satellites around red primaries tended to align with the *major axis*. This finding contrasts sharply with the polar distribution inferred by both Holmberg (1969) and ZSFW.[1] Yang et al. (2006) (hereafter Y06), Azzaro et al. (2007) (hereafter APPZ) and Agustsson & Brainerd (2007) (hereafter AB07) detected a similar anisotropy of satellites in the SDSS; Y06 used over 16 000 groups of galaxies selected to lie within the same dark matter halo, while APPZ and AB07 studied satellites of isolated galaxies; intriguingly, the latter study found that the isotropic distribution around blue galaxies was composed of a *major-axis* alignment for satellites at small projected radii and a *minor-axis* alignment for satellites at large projected radii. Brainerd (2005) (hereafter B05) also selected satellites of isolated galaxies in the SDSS (her largest sample contained approximately 3000 satellites around 2000 primaries) and found that they exhibited a major-axis distribution. Similar results were obtained by Faltenbacher et al. (2007) and Wang et al. (2008), who examined members of tens of thousands of groups in the SDSS. Finally, Azzaro et al. (2006) (hereafter AZPK) found no evidence for anisotropy based on a smaller sample of 193 satellites of 144 isolated late-type galaxies in the SDSS.

These results, derived from both 2dFGRS and SDSS, would seem to suggest that the preferential alignment of satellites about the poles of their primaries noted by both Holmberg (1969) and ZSFW was a consequence of small-number statistics. However, the spatial anisotropy reported by ZSFW was detected with a statistical confidence greater than 99 per cent, suggesting that small-number statistics were unlikely to be a problem. Furthermore, as we have already noted, there is strong evidence for the preferential alignment of satellites about the pole of the Milky Way and evidence

[1] Note that this is opposite to the original claims of SL04 (see the discussion in Y06 for further details).

for subsamples of satellites lying in inclined discs around M31, systems for which we can be certain that the satellites are physically associated with their primaries and for which we know their spatial distribution. Both of these observations raise the spectre that systematic rather than random errors more strongly affect the detection of spatial anisotropies in the distribution of satellites around external galaxies. This leads us to the issue of sample selection.

In the case of both the Milky Way and M31, we have an abundance of detailed information that allows us to state with confidence which galaxies can be considered satellites belonging to these hosts. In the case of external galaxies, we do not have such detailed information and so we must employ selection criteria that allow us to identify which faint galaxy neighbours in projection are likely to be satellites of the primary. Differences arising from how satellite galaxies are selected will affect the measurements of the angular distribution of satellites, and will therefore influence how these data are interpreted.

To illustrate this point, we know that the member galaxies of groups and clusters tend to cluster about the major axis of the brightest group or cluster galaxy (BGG and BCG, respectively; e.g. Binggeli 1982; West 1989; Mandelbaum et al. 2006). If we identify these group or cluster members as satellites of their primary galaxy, the BGG or BCG, then we would interpret this measurement as showing that group or cluster members preferentially align with their primary's major axis. However, we do not expect groups or clusters to be dynamically relaxed and so satellites in these systems might not trace the potential of an equilibrium mass distribution. Therefore, the study of satellites around *isolated* galaxies must be highly successful at excluding such groups and clusters. The ability of selection criteria to identify the proper type of system and to suppress contamination is essential for the result to be considered robust and physical.

Mock galaxy catalogues constructed from cosmological *N*-body simulations provide a powerful method for assessing the reliability of selection criteria. Dark matter haloes are populated with mock galaxies following either a statistical approach based on 'halo occupation distributions' (HOD; e.g. Berlind & Weinberg 2002) or a physically motivated approach based on semi-analytical galaxy formation models (e.g. Cole et al. 2000). Both approaches are parametrized and so statistical properties of the mock galaxy population, such as the luminosity function and the two-point correlation function, are fine-tuned to recover the observed properties of real galaxies in the 2dFGRS and the SDSS. This provides an ideal test bed for selection criteria. We adopt the 'conditional luminosity function' (CLF) formalism of Yang, Mo & van den Bosch (2003), a statistical approach based on HODs, to develop our suite of mock catalogues. The CLF formalism allows us to assign to each dark matter halo in a cosmological *N*-body simulation a probability of hosting N galaxies with a total luminosity L, and a distribution of luminosities drawn from a Schechter function whose parameters depend on the halo mass M. Further details are presented in Section 2.3.

We note that previous studies have used mock galaxy catalogues derived from the CLF formalism to investigate the radial distribution (van den Bosch et al. 2005) and kinematics (van den Bosch et al. 2004) of satellite galaxies. However, we use our mock catalogues to establish *optimal selection criteria* that preferentially pick out *isolated systems* of primary galaxies and their satellites. We explore the impact of different selection criteria on the nature of satellite samples (e.g. group or cluster members?) and to establish robust criteria that minimize the influence of interlopers and a primary's larger scale environment. This allows us to assess selection criteria adopted in previous studies and to quantify the ability of these criteria to identify isolated systems.

By taking such care in establishing the criteria by which our isolated systems are selected, we are able to address a number of important outstanding physical questions using a *robust* sample of galaxies taken from the SDSS. In particular, we revisit the question of whether or not the angular distribution of satellite galaxies about their primary is anisotropic and if anisotropy is linked to the morphological type of the primary. Such dependence would present an exciting possibility to study the connection between subhaloes, haloes and galaxy morphology. In Section 5, we discuss the physical significance of our results in this context.

We also note natural overlaps with studies that seek to measure the flattening of dark matter haloes. There is good evidence to suggest that the haloes of early-type galaxies are flattened along the minor axis of the light – based on studies of X-ray isophotes (e.g. Buote et al. 2002) and weak lensing (e.g. Hoekstra, Yee & Gladders 2004) – whereas the results for disc galaxies are inconclusive. For example, the tidal stream of the Sagittarius Dwarf has been used to infer that the Milky Way's halo is spherical (Ibata et al. 2001; Fellhauer et al. 2006), flattened in the same sense as the disc (Martínez-Delgado et al. 2004; Johnston, Law & Majewski 2005) or, in the opposite sense (Helmi 2004), depending on which part of the stream is modelled (Law, Johnston & Majewski 2005). We discuss the implications of our results for halo flattening in Section 5.

The structure of this paper is as follows. In Section 2, we discuss the sample selection criteria and present our sample of satellites of isolated galaxies. In Section 3, we present our results for the anisotropic distribution of satellite galaxies with respect to their primary galaxy, large-scale filaments and the relative alignment of isolated galaxies with large-scale filaments. In Section 4, we compare our results to previous studies and analyse how different selection criteria provide constraints on the origin of satellite anisotropy. Finally, we discuss the interpretation of the results in terms of the shapes of dark matter haloes, anisotropic infall and the formation of galactic discs in Section 5.

2 SAMPLE SELECTION

The most critical part of the analysis is the process of selecting satellite galaxies of isolated primaries. We must simultaneously do the following:

(i) minimize the number of primaries that are not isolated, i.e. which do not dominate the dynamics of their environment.

(ii) minimize the number of 'interlopers' or satellite-primary pairs that do not represent physical satellites of the primary galaxy.

(iii) maximize the sample size, subject to the above constraints.

We use mock catalogues generated from cosmological simulations to refine our criteria to fulfil the above requirements and critically examine the selection criteria that have been used in previous studies.

2.1 Observational data

2.1.1 SDSS

Our sample is drawn from the SDSS Data Release 6 (DR6) (Adelman-McCarthy et al. 2008). All primary survey objects classified as galaxies in the imaging data that satisfy the spectroscopic targeting algorithm of either the main galaxy sample (Strauss et al. 2002) or the Luminous Red Galaxy sample (Eisenstein et al. 2001)

are considered. Only galaxies with valid spectroscopic redshifts (sciencePrimary = 1 and zConf > 0.85) that are also spectroscopically classified as galaxies are considered as primary or satellite galaxies; however, galaxies without such spectra or which are spectroscopically classified as stars (which often indicates that a foreground star appears near the centre of a galaxy in projection) are also used when evaluating the isolation criteria. We have excluded all objects with unrealistic colours (differences between successive bands of at least 5 mag), as this always indicates a spurious detection at the magnitudes we consider. Petrosian magnitudes are used throughout, and are dereddened using the corrections in Schlegel, Finkbeiner & Davis (1998) and k-corrected using KCORRECT v4_1_4 (Blanton et al. 2003) to the $^{0.1}r$ band[2] to minimize the effect of errors in the *k*-correction. The nominal survey limit for spectroscopic targets in the SDSS main galaxy sample is $r \leq 17.77$; however, the actual limit varies across the sky. Therefore, we conservatively treat it as only being complete to $r \leq 17.5$, although we make use of galaxies as faint as $r = 17.77$ when they are available. When we require photometric redshifts, we use the D1 neural network photometric redshifts available in the SDSS DR6 catalogue (Oyaizu et al. 2008), which are the most accurate available for the $r < 18$ galaxies that we consider. Angular diameter distances and distance moduli are calculated assuming $\Omega_{\rm m} = 0.3$ and $\Omega_\Lambda = 0.7$, and are quoted in *h*-independent units, where $H_0 = h\,100\,{\rm km\,s^{-1}\,kpc^{-1}}$.

2.1.2 *Galaxy classification*

It is important to separate spheroid-dominated early-type galaxies from disc-dominated late-type galaxies. The major axes of spheroidal galaxies are determined by their anisotropic velocity dispersions while those of disc galaxies are determined by their angular momentum; therefore, their orientation with respect to the dark matter halo may be different. Furthermore, the dynamical effects of discs versus spheroids on satellite orbits may be different. Galactic orientations may also depend on their history, which is probed by their stellar populations. Indeed, many previous studies have found that the satellites around red and blue galaxies are distributed differently.

We adopt the galaxy classification scheme of Bailin & Harris (2008b), which is based on the global concentration of the light profile and the location of the galaxy on the colour–magnitude diagram. This method explicitly accounts for inclination effects, and has been validated using high-quality imaging data from the Millennium Galaxy Catalogue (Liske et al. 2003). Galaxies congregate in three distinct regions of parameter space: early-type galaxies are red, highly concentrated and ellipsoidal; intermediate-type galaxies are red, have intermediate concentrations and contain discs; and late-type galaxies are blue, have low concentrations and are disc-dominated. Determining whether the satellite systems of intermediate-type galaxies bear closer relation to those of early- versus late-type galaxies will provide useful insights into their nature.

An analysis of the results when other classification schemes are adopted is given in Appendix C. We find that our qualitative results are unchanged for any reasonable method of splitting the sample, although the numerical magnitude of the effect can vary by $\sim 1\sigma$ depending on the classification method.

[2] The *r* band redshifted to $z = 0.1$; for simplicity we use the notation M_r to refer to $M_{0.1_r}$.

2.2 Definition of selection criteria

The format of our selection criteria is based on Norberg, Frenk & Cole (2008) and is similar to that used in previous studies; however, the details differ in several important ways. To be considered isolated, primaries must not have any comparably bright neighbours within a large surrounding region, and must be much brighter than all the potential satellites in the immediate vicinity. We define three cylinders around each potential primary (see Fig. 1).

(i) Outer isolation cylinder: all galaxies within a projected separation of $\Delta R \leq R_{\rm outer}$ and a velocity difference of $|\Delta v| \leq v_{\rm outer}$ must be at least $m_{\rm outer}$ magnitudes fainter in *r*.

(ii) Inner isolation cylinder: all galaxies within a projected separation of $\Delta R \leq R_{\rm inner}$ and a velocity difference of $|\Delta v| \leq v_{\rm inner}$ must be at least $m_{\rm inner}$ magnitudes fainter in *r* ($m_{\rm inner} > m_{\rm outer}$).

(iii) Satellite cylinder: satellites are galaxies within a projected separation of $\Delta R \leq R_{\rm sat}$ and a velocity difference of $|\Delta v| \leq v_{\rm sat}$. Satellites must be at least $m_{\rm sat}$ magnitudes fainter in *r*. For our criteria, we enforce $R_{\rm sat} = R_{\rm inner}, m_{\rm sat} = m_{\rm inner}$ and $v_{\rm sat} = \frac{1}{2} v_{\rm inner}$.

The adopted values of the parameters are given in Table 1. To ensure that satellites are not associated with more than one primary (a situation we refer to as a 'multi-homed' satellite) and that there are no near neighbours too luminous to be satellites, it is important that $R_{\rm inner} \leq \frac{1}{2} R_{\rm outer}$, $v_{\rm inner} = v_{\rm outer}$, $R_{\rm sat} \leq R_{\rm inner}$, $v_{\rm sat} \leq \frac{1}{2} v_{\rm inner}$ and $m_{\rm sat} = m_{\rm inner}$. These sanity checks are not fulfilled by many of the criteria that have been used in the previous studies.

We also apply the following additional criteria.

(i) All primaries must be at least $m_{\rm inner}$ magnitudes brighter than $r = 17.5$ to ensure that all potential bright neighbours are brighter than the local survey limit.

(ii) The projected distance from the primary to the nearest edge of the photometric survey footprint must be at least $R_{\rm outer}$ to ensure that any potential bright neighbours have been observed photometrically. The projected distance from the primary to the nearest edge of the spectroscopic survey footprint must be at least $R_{\rm sat}$ to ensure that all potential satellites are equally likely to have been observed spectroscopically, and therefore that the survey edge does not impose an angular bias in the selected satellite population.

(iii) Because of the spectral incompleteness, ∼10 per cent of galaxies that fulfil the requirements of the SDSS main galaxy targeting criteria do not have observed redshifts. Therefore, there are potential primaries that would not be considered isolated if it turned out that their non-spectroscopic neighbours are at the same redshift. This issue is particularly important because the limited number of fibres per tile causes the fractional completeness to be lower in regions of high galactic density. There are a number of ways of treating such galaxies (hereafter referred to as 'violators'): one could assume that most do not lie at the same redshift as the primary and simply ignore their presence (SL04; B05; AZPK; APPZ; Y06; AB07), one could establish a threshold such that if there are more than a number $N_{\rm viol}$, then the chances that at least one is at the same redshift as the primary is high and therefore eliminate those primaries (Herbert-Fort et al. 2008; Norberg et al. 2008) or one could eliminate all such primaries on the grounds that there is a chance that they are not isolated (equivalent to setting $N_{\rm viol} = 0$; ZSFW). The existence of photometric redshifts in the SDSS DR6 catalogue allows us to use a more sophisticated method of determining whether the violators are likely to be at the same redshift as the primary. We first check the NASA/IPAC Extragalactic Data

Table 1. Parameters of selection criteria.

Parameter	This work	ZSFW	SL04	B05			AZPK	APPZ		AB07
				S1	S2	S3		S1	S2	
Outer isolation cylinder										
$R_{\rm outer}(h^{-1}\,{\rm kpc})$	1000	750	...	...	...	700	...	...	...	...
$v_{\rm outer}({\rm km\,s^{-1}})$	1500	1000	...	...	...	1000	...	...	...	...
$m_{\rm outer}$	0.7	0.7	...	...	...	0.7	...	...	...	...
Inner isolation cylinder										
$R_{\rm inner}(h^{-1}\,{\rm kpc})$	500	375	700	490	2000	350	500	490	500	511
$v_{\rm inner}({\rm km\,s^{-1}})$	1500	1000	1000	1000	1000	1000	1000	1000	1000	1000
$m_{\rm inner}$	2.0	2.2	1.0	1.0	0.7	2.2	2.0	1.0	2.0	1.0
Satellite cylinder										
$R_{\rm sat}(h^{-1}\,{\rm kpc})$	500	375	500	350	350	350	350	350	350	365
$v_{\rm sat}({\rm km\,s^{-1}})$	750	500	500	500	1000	500	500	500	500	500
$m_{\rm sat}$	2.0	2.2	2.0	2.0	1.5	2.2	2.0	2.0	2.0	2.0
$N_{\rm viol}$	NED+photo-z^a	0^a	...	...	...	...	...	...	...	...
$f_{\rm sat}$	0.2	...	...	1.0	1.0	1.0	...	...	...	1.0
$N_{\rm satmax}$	4	...	4	...	...	...	...	...	...	9
Sanity checks										
Forbids multihomed satellites[b]	Yes	Yes	No	No	No	Yes	Yes	No	Yes	No
Forbids nearby non-satellites[c]	Yes	Yes	No	No	No	Yes	Yes	No	Yes	No
Avoids survey edge[d]	Yes	N/A	No	No	No	No	Yes[a]	No	No	Yes
Avoids survey magnitude limit[e]	Yes	Yes	No	No	No	No	Yes	No	Yes	No

[a] See text for further clarification.
[b] The criteria do not permit satellites to belong to more than one primary galaxy.
[c] The criteria do not permit there to be bright (non-satellite) galaxies within the satellite cylinder.
[d] The criteria do not permit primaries so near the edge of the survey that potential bright neighbours would lie outside the survey region.
[e] The criteria do not permit primaries faint enough that potential bright neighbours fall below the local survey magnitude limit.

base (NED[3]) for literature spectroscopic redshifts of the violators of all primaries that would otherwise be included in our sample. If no spectroscopic redshift is available, then we consider the photometric redshift $z_{\rm viol,photo}$; if it is within $2\sigma_{\rm viol,photo}$ of the spectroscopic redshift of the primary, where $\sigma_{\rm viol,photo}$ is the estimated error on the photometric redshift in the catalogue, then we eliminate the primary. We ignore the presence of violators that do not exist in the photometric redshift data base, as these are mostly galaxies that are not detected in one or more bands; such galaxies are highly unlikely to be truly bright physical neighbours of the relatively luminous nearby galaxies that constitute our sample of primary galaxies. We have confirmed that excluding primaries with such neighbours does not alter our conclusions.

(iv) The total luminosity of the satellites must not be more than $f_{\rm sat}$ times the luminosity of the primary, and systems with more than $N_{\rm satmax}$ satellites are discarded. This ensures that the primary galaxy dominates the satellite system.

(v) Postage stamp images of each potential primary were examined by eye. 11 objects were removed, four of which suffered from the catastrophically bad background subtraction due to nearby bright objects and seven of which are major mergers in progress.

Our choices for the relevant parameters are motivated by the analysis using mock catalogues as described in Section 2.3.4. Where applicable, the values previous authors have used for the selection parameters are given in Table 1. For those criteria that use only one isolation cylinder, we characterize it as an 'Inner' cylinder. We summarize the selection criteria used by each previous study below.

ZSFW used somewhat thinner and shorter cylinders than those used in this work, but the criteria fulfil the above sanity checks. They did not have redshifts and magnitudes for every galaxy in the field, but eliminated all primaries that appeared by eye to have potentially criteria-violating neighbours (i.e. $N_{\rm viol} = 0$). There was no formal edge of the surveyed area, and primaries were chosen to be at least 2.5 mag brighter than the Palomar Observatory Sky Survey (POSS) magnitude limit, so all potential bright neighbours were considered. No cut on the number or luminosity fraction of satellites was imposed, and only morphological late-types were included as primaries.

SL04 used only one isolation cylinder, which did not satisfy $m_{\rm sat} \leq m_{\rm outer}$. Therefore relatively bright galaxies are allowed to be in the satellite region. Because of this definition, satellites may be multihomed. Only primary galaxies with absolute magnitude $M_{b_J} - 5\log h < -18$ were used. They did not impose any constraints on proximity to the survey magnitude limit, proximity to the survey edge $N_{\rm viol}$, or $f_{\rm sat}$, but used $N_{\rm satmax} = 4$.

B05 tested three selection criteria; her Sample 1 (S1) used isolation criteria based on SL04 (though adopting a different value of the Hubble constant); her Sample 2 (S2) used one very wide isolation cylinder, which permits bright galaxies to be in the satellite region and satellites to be multihomed, and her Sample 3 (S3) used isolation criteria based on ZSFW (though adopting a different value of the Hubble constant). There was no cut on proximity to the survey edge, $N_{\rm viol}$, or $N_{\rm satmax}$ in any of the samples. There was a cut on $f_{\rm sat}$ of 1.0.

AZPK used Sample 2 of Prada et al. (2003), but restricted the primaries to be morphological late-types, adopted a redshift limit of $cz \leq 11\,000\,{\rm km\,s^{-1}}$, and only examined primaries with $-20.5 \leq M_B \leq -19.5$. These criteria are similar to SL04, except that because $m_{\rm sat} = m_{\rm outer}$, the satellite cylinder is not permitted to contain bright galaxies, and satellites can only belong to a single primary. Although they did not formally adopt a cut on proximity to the survey edge, they searched for bright neighbours in de Vaucouleurs et al. (1991) (hereafter RC3), which fulfils the same purpose. The narrow range

[3] http://nedwww.ipac.caltech.edu/

of absolute magnitudes and redshift limit serves the same purpose as our cut on galaxies near the survey magnitude limit. They did not make any cut on $N_{\rm viol}, N_{\rm satmax}$ or $f_{\rm sat}$.

APPZ tested two sets of criteria. Their Sample 1 (S1) used the same criteria as B05 S1 but without the cut on $f_{\rm sat}$. Their Sample 2 (S2) is identical to AZPK except that a wider range of primary luminosities, $-23 \leq M_r \leq -21$ is used, the redshift limit is extended to $cz \leq 30\,000\,{\rm km\,s^{-1}}$ and no check for bright neighbours outside of the survey boundary is performed.

AB07 used the criteria very similar to B05 S1, but they adopted a slightly different value for the Hubble constant, restricted $N_{\rm satmax}$ to nine and ensured that their primary galaxies were not near the edge of the spectroscopic survey.

Holmberg (1969) did not have redshifts for any of his galaxies, making it difficult to directly compare our selection. It is also difficult to compare our selection with Y06 or Faltenbacher et al. (2007), who used an iterated percolation algorithm rather than isolation criteria. Their selections were tuned using mock catalogues to minimize the number of interlopers; however, they were not designed to find isolated galaxies and most of their systems should be considered groups or clusters rather than satellite systems of isolated galaxies.

Our criteria are more restrictive than other criteria that have been used to select isolated galaxies. The advantage of using such a large sample as SDSS DR6 is less the ability to boost the statistics than the ability to be extremely conservative with our selection criteria and still retain an acceptable number of galaxies. Given that the disagreement between previous results is more likely due to systematic errors than statistics, such a rigorous treatment is essential to disentangling the nature of the disagreement and determining the true distribution.

2.3 Mock catalogues

2.3.1 The conditional luminosity function $\Phi(L|M)$

We construct our mock galaxy catalogues following the prescription presented in Yang et al. (2004) (hereafter Y04), which is based on earlier studies by Yang et al. (2003) and van den Bosch, Yang & Mo (2003). This approach allows us to assign to each dark matter halo of mass M a probability of hosting a population of N galaxies of total luminosity L. This probability is governed by the conditional luminosity function (CLF), $\Phi(L|M)$, which is parametrized by the Schechter function,

$$\Phi(L|M){\rm d}L = \frac{\tilde{\Phi}^*}{\tilde{L}^*}\left(\frac{L}{\tilde{L}^*}\right)^{\tilde{\alpha}} \exp(-L/\tilde{L}^*)\,{\rm d}L. \quad (1)$$

The normalization $\tilde{\Phi}^*$, characteristic luminosity $\tilde{L}^*$ and faint-end slope $\tilde{\alpha}$ are all functions of halo mass M; appropriate expressions for these quantities are in Appendix A.

Given $\Phi(L|M)$, we compute the following various 'observable' properties of the galaxy population associated with an average dark matter halo of mass M:

(i) the mean number of galaxies $\langle N\rangle$ (M) (see equation B1);

(ii) the luminosities of the central galaxy $L_{\rm cen}$ and satellite galaxies $L_{\rm sat}$ (see equation B3);

(iii) the morphological type of each galaxy (i.e. early- versus late-type; see Appendix B).

All of these properties can be recovered using analytic dark matter halo mass functions, but a cosmological N-body simulation is required to assign phase-space coordinates to mock galaxies. In what follows, we briefly describe the main steps involved in constructing the mock catalogues. A more detailed description is provided in Appendix B.

Table 2. Cosmological N-body simulations. $L_{\rm box}$ refers to the length of the simulation box; $m_{\rm part}$ is the particle mass, which depends on both $L_{\rm box}$ and the number of particles $N_{\rm part}$; ϵ is the gravitational force softening; $M_{\rm min}$ is a (conservative) estimate of minimum halo mass that can be reliably resolved, based on convergence of the mass function, and $L_{\rm min}$ is the minimum luminosity.

$L_{\rm box}$ (h^{-1} Mpc)	$m_{\rm part}$ ($h^{-1}\,{\rm M}_\odot$)	ϵ (h^{-1} kpc)	$M_{\rm min}$ ($h^{-1}\,{\rm M}_\odot$)	$L_{\rm min}$ ($h^{-2}\,{\rm L}_\odot$)
35	0.21×10^9	2.7	10^{10}	1.1×10^8
50	0.62×10^9	3.9	3×10^{10}	1.1×10^8
70	1.7×10^9	5.5	9×10^{10}	1.1×10^9
100	4.96×10^9	7.8	25×10^{10}	1.1×10^9

2.3.2 Populating dark matter haloes with galaxies

We perform a series of cosmological N-body simulations following the formation of structure in a Λ cold dark matter (CDM) model from $z = 50$ to 0. Each simulation contains 256^3 particles. We adopt cosmological parameters of $\Omega_{\rm m} = 0.3, \Omega_\Lambda = 0.7$ and $h = 0.7$, and the power spectrum of initial density perturbations (generated using CMBFAST; Seljak & Zaldarriaga 1996) is normalized assuming a mass variance of $\sigma_8 = 0.9$. Details of the runs are presented in Table 2. We quote results using the five $100\,h^{-1}$ Mpc boxes (labelled as 'A' through 'E'), but have verified using the smaller boxes that this resolution is sufficient to reproduce the statistical properties of the mock catalogues.

These simulations provide the dark matter host haloes that we populate with mock galaxies. Haloes are identified at $z = 0$ using the friends-of-friends (FOF) algorithm with a linking length of $b = 0.2$ times the mean interparticle separation. For each halo, we compute its virial mass and radius, and also record the coordinates of its most bound particle and a list of all particles that reside within its virial radius. This is (in principle) all the information we need to construct our mock galaxy catalogues.

We note that $\tilde{\Phi}^*$, $\tilde{L}^*$ and $\tilde{\alpha}$ are functions of halo mass M, but they also depend on the cosmological parameters. Yang et al. (2003) presented a number of different CLFs for different cosmologies and different assumptions regarding the free parameters, and we adopt those used by Y04, who assumed a flat ΛCDM cosmology with $\Omega_{\rm m} = 0.3, \Omega_\Lambda = 0.7, h = 0.7$ and a normalization $\sigma_8 = 0.9$. Precise values for the CLF parameters are given in Appendix A.

These parameters were chosen to recover the observed luminosity functions and correlation lengths of galaxies in the 2dFGRS (as a function of both their luminosity and their type), but we find that the clustering and luminosity functions of galaxies in our mock catalogues are in very good agreement with the corresponding SDSS correlation and luminosity functions.

It is important to estimate the minimum reliably resolved halo mass $M_{\rm min}$; below this threshold the number density of haloes tends to be suppressed relative to the number density they would have in the limit of infinite numerical resolution. In this work, we assume that the mass function is converged for haloes containing 50 particles or more (see discussion in Appendix B); this gives $M_{\rm min} = 50\,m_{\rm part}$ in Table 2.

Knowing $M_{\rm min}$ allows us to estimate $L_{\rm min}$, the minimum luminosity that we can assign to a mock galaxy, using the 'conditional

probability distribution' $P(M|L)$. $L_{\rm min}$ fixes the halo occupation number, the average number of galaxies per halo of mass M, $\langle N\rangle\,(M)$ (equation B1); as $M_{\rm min}$ and therefore $L_{\rm min}$ decreases (increases), $\langle N\rangle\,(M)$ decreases (increases). The mass resolution of our simulations means that we adopt $L_{\rm min} = 1.1 \times 10^9\,h^{-2}\,{\rm L}_\odot$ in our mock catalogues A to E, upon which our analysis is based.

We assume that the number of galaxies N in a dark matter halo is Poisson distributed about $\langle N\rangle\,(M)$ (Yang et al. 2003) and that each galaxy is assigned a luminosity drawn from $\Phi(L|M)$. The central galaxy is defined to be the brightest galaxy in the halo and has a luminosity $L > L_1$, where L_1 satisfies the condition that $\langle N\rangle\,(M) = 1$ (see equation B3). The remaining $N-1$ galaxies have luminosities that are drawn randomly from the luminosity function in the range $L_{\rm min} < L < L_1$.

The morphological type of each galaxy is obtained from $f_{\rm late}(L, M)$ (equation B4), the probability that a galaxy of luminosity L hosted by a dark matter halo of mass M is late-type. Finally, the position and velocity of the central galaxy are associated with those of the most bound particle in the halo, while the positions and velocities of the remaining $N-1$ galaxies are obtained by randomly sampling the particles in the FOF group.

A more detailed description of our approach to populating dark matter haloes with galaxies is given in Appendix B.

2.3.3 *Constructing a mock galaxy redshift survey*

At this point, we depart from Y04, who wished to study a mock 2dFGRS and stacked simulation boxes to recover the survey's median redshift. Our needs are more modest – we wish to evaluate the reliability of our sample selection criteria. To transform our raw mock galaxy distribution into a mock galaxy catalogue, we do the following.

(i) We select a single simulation box, recalling that each box has periodic boundary conditions, and replicate it thrice along each dimension, producing a stack of $3 \times 3 \times 3$ boxes. We then centre the stacked boxes on the median redshift of the SDSS $z_{\rm med} = 0.11$.

(ii) We place a virtual observer at $z = 0$ and define an (α, δ) coordinate frame with respect to the centre of the stacked box.

(iii) We compute a redshift z for each galaxy as seen by the virtual observer from the recessional velocity $cz = Hr + \boldsymbol{v}\cdot\boldsymbol{r}/|r|$, where the galaxy is at $\boldsymbol{r}$ with respect to the virtual observer and $\boldsymbol{v}\cdot\boldsymbol{r}/|r|$ is its line-of-sight velocity. We account for observational velocity uncertainties by adding a random velocity drawn from a Gaussian of width $30\,{\rm km\,s^{-1}}$. We also compute the apparent magnitude according to its luminosity and distance, to which we add a rms error of 0.02 mag, in accordance with the SDSS internal estimates of the redshift and photometric errors for galaxies.

(iv) We remove the redshifts of all galaxies that fall below the magnitude limit, $r = 17.77$, of the SDSS main galaxy sample and those with declinations less than $+30^\circ$, for which the depth of the stacked simulation boxes is insufficient and which we define as the edge of the mock survey boundary.

There are a number of attributes of the observed survey that are not accurately reproduced by the mock survey. The true survey boundary is much more complicated than the boundary of our mock catalogue, and hence a much larger fraction of galaxies lie near an edge and may be near an unseen bright galaxy. Also, the true survey is not spectroscopically complete, and is less complete in the regions of higher density due to the lower availability of fibres. Therefore, our analysis using the mock catalogues would underestimate the importance of excluding primaries near the survey edge, excluding primaries near the magnitude limit of the survey and implementing a cut based on $N_{\rm viol}$. As these issues cannot be addressed well using the mock catalogues, we do not implement them in our analysis of the mock catalogue. Their effects on the sample are investigated empirically in Section 3.1.

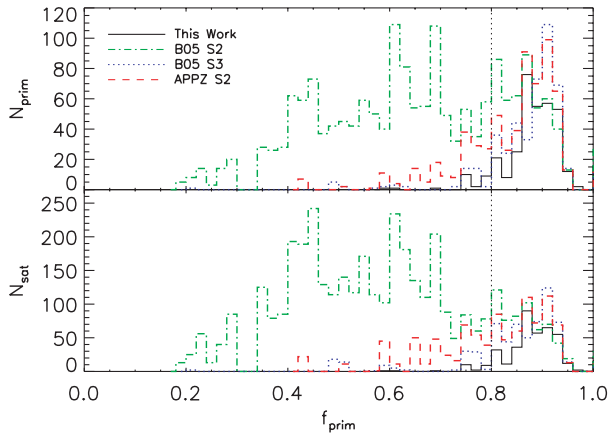

Figure 2. Top panel: histogram of the number of primaries selected from the mock catalogue as a function of $f_{\rm prim}$, the fraction of the true halo luminosity that comes from the primary galaxy. The solid lines represent systems chosen using our adopted selection criteria, while the other line styles indicate other representative criteria (dot–dashed, dotted and dashed for B05 S2, B05 S3 and APPZ S2). Bottom panel: as above, but weighted per satellite in the sample. The vertical dotted lines denote the $f_{\rm prim}$ below which primaries are considered non-dominant.

2.3.4 *Tests of our selection criteria*

Using the mock catalogues, we quantify the degree to which current and previous selection criteria accurately identify physical satellites of isolated galaxies. We quote the results of the 'Mock A' catalogue (see Table D1), but the results are consistent with those from the other mock catalogues.

Interlopers are identified in the mock catalogues as satellites that do not belong to the same halo as their selected primary galaxy.[4] We do not consider primary galaxies as isolated if

(i) they are not the central galaxy of their halo or
(ii) they are not sufficiently more massive than other galaxies within the halo.

Point (i) is easily determined from the mock catalogues because we know which galaxy is the central galaxy of each halo. Point (ii) is more difficult to determine because the CLF formalism assigns luminosities and not masses to individual galaxies. However, we can estimate the degree to which the primary galaxy dominates its halo by calculating the fraction of the total halo luminosity that is contributed by the primary galaxy,

$$f_{\rm prim} \equiv L_{\rm prim}/L_{\rm tot}. \qquad (2)$$

In the top panel of Fig. 2, we plot a histogram of the number of selected primaries as a function of $f_{\rm prim}$ for four sample sets of

[4] Note that many previous works refer to all unwanted satellites as 'interlopers', regardless of the reason for wanting to exclude them from the sample. We prefer to designate only satellites that are not physically associated with their selected primary as 'interlopers' to distinguish them from satellites that are physically associated with unwanted primaries.

Table 3. Results of applying selection criteria to mock catalogues.

Parameter	This work	ZSFW	SL04	B05			AZPK	APPZ		AB07
				S1	S2	S3		S1	S2	
Selected primaries	337	135	1516	1828	1778	404	114	1595	636	589
Non-central primary fraction	0.000	0.007	0.001	0.002	0.002	0.002	0.000	0.003	0.000	0.005
Non-dominant primary fraction	0.071	0.059	0.600	0.640	0.724	0.087	0.123	0.656	0.272	0.626
Isolated primary fraction	0.929	0.941	0.400	0.360	0.276	0.913	0.877	0.344	0.728	0.374
Selected satellites	388	187	2396	3461	3852	563	133	3081	980	1112
Multihomed fraction	0.000	0.000	0.000	0.000	0.001	0.000	0.000	0.000	0.000	0.000
Interloper fraction	0.046	0.048	0.037	0.036	0.038	0.025	0.023	0.042	0.036	0.049
$f_{\rm non-dom}$	0.062	0.102	0.691	0.767	0.844	0.151	0.218	0.778	0.409	0.754
Correctly selected satellite fraction	0.892	0.861	0.290	0.216	0.138	0.824	0.759	0.203	0.563	0.224

criteria (ours, B05 S2, B05 S3 and APPZ S2) that span the range of observed behaviours. In the bottom panel, we weight each primary by its number of selected satellites to demonstrate its influence on the observed sample. Because primaries that contribute less to the luminosity of their halo have more satellites, the tail to low fractions is exacerbated. The histograms are characterized by a symmetric peak centred at $f_{\rm prim} = 0.9$ that extends down to 0.8 that we identify as truly isolated primaries, and a long tail to low values that we wish to eliminate. Based on the examination of these histograms, we consider a primary to be 'non-dominant' if $f_{\rm prim} < 0.8$ (denoted by the vertical line in Fig. 2).

Table 3 lists the number of primaries and satellites selected from the mock catalogue that pass and fail the above interloper and isolation criteria. Row 1 indicates the number of primaries selected, row 2 indicates the fraction of those primaries that are not the central galaxy of their halo (category i above), row 3 indicates the fraction of primaries that do not dominate the dynamics of their halo (category ii above) and row 4 indicates the fraction of selected primaries that are truly isolated. Row 5 indicates the number of satellites selected, row 6 indicates the fraction of those satellites that are 'multihomed', i.e. selected as satellites of more than one primary, row 7 indicates the fraction of satellites that do not belong to the same halo as their selected primary ('interlopers'), row 8 indicates the fraction of satellites that are physically associated with non-dominant primaries ('$f_{\rm non-dom}$') and row 9 indicates the fraction of selected satellites that are selected correctly, i.e. they are physically associated with isolated primaries.

When evaluating criteria based on different bandpasses, we use the following simple transformations: for the AZPK criteria, which are based on RC3 B_T magnitudes, we assume a constant $B - {}^{0.1}r = 0.6$, typical of the late-type galaxies they studied; for the APPZ criteria, we assume a constant difference between the $z = 0$ and $z = 0.1$ r-band k-corrections of 0.23 mag and for the SL04 criteria, which are based on UK Schmidt b_J magnitudes, we assume a constant $b_J - {}^{0.1}r = 0.7$, intermediate between the typical values for early- and late-type galaxies.

The use of the mock catalogues to evaluate selection criteria for studies that did not use SDSS data is not as accurate as for those studies based on SDSS because the parameters of the mock catalogues, such as the typical photometric and redshift error, are specifically tuned to mimic SDSS. The photometric errors in ZSFW and the velocity errors in SL04 are significantly larger.

All sets of criteria do an adequate job of selecting central galaxies as primaries and minimizing the fraction of interlopers and multihomed satellites, with each source of contamination contributing less than 5 per cent to each sample.[5] However, the fraction of the sample that lies around non-dominant primaries ($f_{\rm non-dom}$) extends from a low of 6 per cent for our adopted criteria to almost 85 per cent in the case of B05 S2. We have examined by eye the fields surrounding a subset of the primary galaxies in our SDSS sample in order to confirm that this is an accurate measure of the degree of isolation of the sample, and estimate that 7 per cent of our primaries are members of groups, in very good agreement with the value that we derive from the mock catalogues.

The greatest single predictor of the magnitude of $f_{\rm non-dom}$ is whether non-satellites are permitted to lie within the satellite cylinder. In other words, criteria with $m_{\rm sat} > m_{\rm inner}$ generally fail to select isolated primaries. Although we do not evaluate the effects of $N_{\rm viol}$ using the mock catalogues, neglecting to account for spectroscopic incompleteness is the other factor that can result in galaxies larger than satellites lying within the satellite cylinder; we therefore expect that this also has a significant effect on $f_{\rm non-dom}$. The impact of non-dominant primaries on the results will be discussed in detail in Section 4.

One might ask how sensitive these conclusions are to the CLF method used to assign luminous galaxies to dark matter haloes versus, for example, a semi-analytic model. Motivated by the halo luminosity function found in a particularly discrepant semi-analytic model of Eke et al. (2004, their fig. 5), we have tested a mock catalogue where we arbitrarily doubled the luminosity of the central galaxy. The resulting $f_{\rm non-dom}$ changes by less than 0.1 for the vast majority of selection criteria tested. Given the insensitivity of $f_{\rm non-dom}$ to such relatively dramatic departures from our method of assigning luminous galaxies to dark matter haloes, we feel confident that our conclusions regarding the selection criteria used in previous studies are robust.

We have optimized the parameters we use for the selection criteria using the mock catalogues to maximize both the size of the sample (row 5) and the fraction of the sample that passes all of the checks (row 9). In particular, all parameters in Table 1 were varied in turn and the new value was kept if it increased the sample size without a correspondingly large increase in the incorrectly selected fraction (the inverse of the value in row 9), the interloper fraction or the fraction of satellites around non-dominant primaries; or, conversely, if it decreased the incorrectly selected fraction without a correspondingly large decrease in sample size. When in doubt,

[5] Although it is in principle possible to select multihomed satellites using many of the sets of criteria, only for B05 S2 does this situation ever occur in practice.

we erred on the side of more restrictive criteria. This process was repeated until convergence.

2.4 The sample

The following quality cuts are imposed on the sample.

(i) Satellites within $35\,h^{-1}$ kpc of the primary are removed due to the known sky subtraction problem around bright sources (Mandelbaum et al. 2005, 2006), and the possibility of bright knots in the outer regions of a galaxy being mistakenly deblended as separate galaxies.

(ii) As the interloper fraction rises at large projected radius, and the radius at which interlopers dominate increases with halo mass, we eliminate satellites of less luminous ($M_r - 5\log h > -21.1$, i.e. fainter than the median) intermediate- and early-type primaries and of all late-type primaries which lie beyond a projected radius of $345\,h^{-1}$ kpc; this choice of parameters is justified below.

The resulting sample of primary and satellite galaxies is given in Table 4. The full sample contains 866 satellites of 722 primaries; 311/138/273 of the primaries are classified as early-/intermediate/late-type hosting 378/167/321 satellites, respectively.

The following cuts are further imposed on systems used to measure the anisotropy around primary galaxies.

(i) Primaries that do not have a measured position angle (PA) in the SDSS DR6 data base are excluded; this cut excludes 11 primaries.

(ii) Primaries with isophotal axis ratios $b/a > 0.8$ are excluded. Galaxies with nearly circular isophotes have poorly constrained PAs. In addition, any anisotropy that exists in three dimensions gets washed out in projection as the system is viewed close to its axis of symmetry. The numerical choice of $b/a > 0.8$ for this cut-off is motivated in Section 3.1 and the effects of changing this value are discussed.

Unless otherwise specified, this subsample is the sample referred to for the remainder of the paper and contains 440 satellites of 372 primaries. In Section 3.2, we analyse the distribution of satellites with respect to the large-scale structure (LSS). For those purposes, the following further cuts are imposed instead.

(i) Systems within a projected radius $3000\,h^{-1}$ kpc of the edge of the spectroscopic survey footprint are excluded in order to ensure that the survey boundary does not introduce a bias in the derived LSS axis.

(ii) Primaries for which the LSS axis is undefined, because there are no galaxies within the cylinder used to define the axis or for which the LSS axis ratio is greater than 0.9, are excluded.

This subsample contains 572 satellites of 480 primaries.

The distribution of luminosities, number of satellites per primary, radial separations and the velocity differences are shown in Fig. 3. In Fig. 3(a), we plot the absolute magnitude distributions of the primary and satellite galaxies, along with the magnitude difference. The median absolute magnitude is $M_r - 5\log h = -21.1$. The typical primary has a luminosity similar to the Milky Way, while the typical satellite is $\sim$2.5 mag fainter, slightly brighter than the Large Magellanic Cloud (LMC). Fig. 3(b) shows the number of satellites per primary. Most primaries are surrounded by only one satellite. Fig. 3(c) presents the distribution of radial separation between satellites and primary galaxies for samples split by the type and luminosity of the primary (the median absolute magnitude, -21.1, is used as the cut-off between the 'bright' and 'faint' subsamples). In this panel only, we include the distant satellites of the faint primaries. The radial distribution of true satellites declines with radius, while the distribution of interlopers increases (Chen et al. 2006). The crossover between these regimes occurs at the edge of the dark matter halo, and therefore depends on galaxy mass. Fig. 3(c) shows no evidence for an increase in the number of outer satellites due to interlopers around bright early- and intermediate-type primaries. However, such an upturn is evident around faint primaries of both morphologies and all late-type primaries beyond $\Delta R > 345\,h^{-1}$ kpc. Therefore, around these primaries, we exclude satellites at projected radii $\Delta R > 345\,h^{-1}$ kpc in all other panels and remaining plots; however, we have confirmed that if we include these satellites, our results are qualitatively unchanged. Fig. 3(d) presents the distribution of velocity differences between satellites and their primaries. The velocities of selected satellites cluster strongly about the velocity of the primary indicating that they are indeed physically associated. The velocity dispersion of satellites around bright primaries is higher than around faint primaries due to their larger mass (see e.g. Conroy et al. 2007; Norberg et al. 2008, and references therein).

3 RESULTS

3.1 Distribution about the primary galaxy

We define the 'disc angle' as the angle between the *r*-band isophotal PA of the major axis of the primary and the PA of the great circle between the primary and satellite (see Fig. 1); we fold this angle into the range 0°–90°. If satellites are distributed isotropically around the primaries, then the distribution of disc angles is uniform with a mean of 45°.

In Fig. 4, we plot the cumulative and differential disc angle distributions. The full sample shows a tendency to lie at small disc angles, i.e. for the satellites to lie near the major axis of their parent galaxy. The hypothesis that the angles are distributed randomly is ruled out at a greater than 2σ level: according to the Kolmogorov–Smirnov (KS) test, the probability is 0.06 with a mean disc angle of $42\overset{\circ}{.}5 \pm 1\overset{\circ}{.}2$.

The satellites surrounding different types of primaries show different angular distributions: there is a clear excess concentration of satellites along the major axis for early-types, hints of a major-axis excess around intermediate-types (the measured magnitude of the anisotropy is in fact larger than around early-types, but is detected at less than 2σ) and no detectable anisotropy around late-types. The mean disc angles are $41\overset{\circ}{.}3 \pm 0\overset{\circ}{.}9$, $40\overset{\circ}{.}5 \pm 2\overset{\circ}{.}5$ and $45\overset{\circ}{.}5 \pm 2\overset{\circ}{.}1$ around early-, intermediate- and late-types, respectively, with KS test probabilities of being drawn from a random distribution of 0.03, 0.10 and 0.99. When the samples are combined, these effects counteract each other, with the isotropic satellites of late-types diluting the major-axis alignment seen around the early-types. The KS test results, the mean and median disc angles and the polar fraction (the fraction of satellites with disc angles larger than 45°) are listed in Table 5. The quoted uncertainties are determined using bootstrap resampling of the primaries and represent 68 per cent of confidence intervals. All statistics reinforce the same conclusion, i.e. satellites of spheroidal early-type galaxies tend to lie near the long axis of the spheroid, while satellites of disc galaxies are isotropically distributed around blue late-types but show hints of lying near the disc around red intermediate-types. We have verified using the mock catalogues, which have intrinsically isotropically distributed satellites that we could not have measured this level of anisotropy

Table 4. Sample of data for primary and satellite galaxies. (The full version of this table is available in the online version of the article. Please see the Supporting Information section for details.)

Primary name[a]	Satellite name[b]	RA[c]	Dec.[d]	z^e	$^{0.1}M_r$[f]	PA[g]	b/a[h]	LSS PA[i]	Class[j]	Disc sample?[k]	LSS sample?[l]
SDSS J155146.83−000618.6	...	15 51 46.8	−00 06 18.6	0.05443	−21.27	128.3	0.93	−50.5	E	...	...
...	SDSS J155151.10−000644.9	15 51 51.1	−00 06 44.9	0.05436	−19.22	150.6	0.79	...	E	N	N
SDSS J140445.89−004909.1	...	14 04 45.9	−00 49 09.1	0.08378	−21.69	104.4	0.68	...	E	...	...
...	SDSS J140513.54−005103.2	14 05 13.5	−00 51 03.2	0.08409	−19.63	10.7	0.37	...	L	Y	N
SDSS J140525.25−004840.8	...	14 05 25.3	−00 48 40.8	0.04927	−21.12	95.7	0.54	−37.1	L	...	...
...	SDSS J140524.17−004734.4	14 05 24.2	−00 47 34.5	0.04923	−19.00	8.2	0.71	...	E	Y	Y
SDSS J141628.95−004437.9	...	14 16 29.0	−00 44 38.0	0.04887	−20.74	173.4	0.51	13.1	I	...	...
...	SDSS J141634.04−003855.9	14 16 34.0	−00 38 55.9	0.04864	−18.60	40.8	0.53	...	L	Y	Y
SDSS J150952.05−002304.9	...	15 09 52.1	−00 23 05.0	0.07116	−22.32	35.5	0.54	10.9	I	...	...
...	SDSS J150933.51−002018.8	15 09 33.5	−00 20 18.8	0.07092	−19.36	149.0	0.68	...	E	Y	Y
...	SDSS J150935.69−002339.3	15 09 35.7	−00 23 39.3	0.07111	−19.48	70.1	0.86	...	E	Y	Y
SDSS J005157.28+143348.3	...	00 51 57.3	+14 33 48.4	0.07775	−21.69	174.8	0.78	−108.5	E	...	...
...	SDSS J005226.85+143239.8	00 52 26.9	+14 32 39.8	0.07751	−19.37	47.6	0.87	...	L	Y	Y
SDSS J013307.54+144539.0	...	01 33 07.5	+14 45 39.1	0.05608	−20.98	153.0	0.67	−105.5	E	...	...
...	SDSS J013224.02+144337.1	01 32 24.0	+14 43 37.1	0.05687	−18.65	101.8	0.23	...	L	N	N

[a]IAU designation of object if it is a primary.
[b]IAU designation of object if it is a satellite.
[c]Right ascension.
[d]Declination.
[e]Redshift.
[f]Absolute dereddened $^{0.1}M_r - 5\log h$ magnitude.
[g]Isophotal PA.
[h]Ratio of isophotal minor and major axes.
[i]Derived PA of the LSS axis.
[j]Classification of galaxy as early-type ('E'), intermediate-type ('I') or late-type ('L') based on the classification scheme of Bailin & Harris (2008b).
[k]Whether the system passes all quality cuts required to be included in the sample for the purposes of measuring the anisotropy with respect to the primary.
[l]Whether the system passes all quality cuts required to be included in the sample for the purposes of measuring the anisotropy with respect to the LSS.

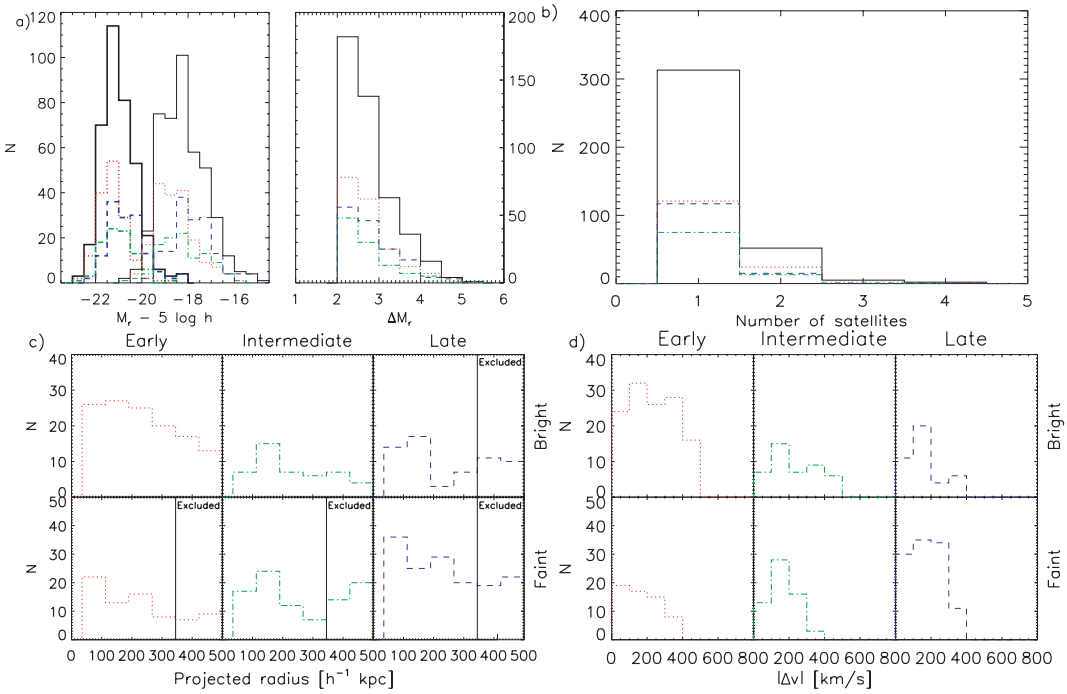

Figure 3. (a) Absolute magnitude distributions of primary galaxies (thick lines) and satellites (thin lines) (left-hand panel), and the difference between the magnitude of each satellite and its primary (right-hand panel). The red/dotted lines show the distribution for early-type primaries, the green/dot–dashed lines show the distribution for intermediate-type primaries and the blue/dashed lines refer to late-type primaries. Note that the satellites are also separated according to the type of their primary, not according to their own type. (b) Distribution of number of satellites per primary. Line colours/styles indicate the classification of the primary galaxy as in (a). (c) Distribution of projected radial separation of satellites from their primary. Left-hand panels show satellites of early-type galaxies, middle panels show satellites of intermediate-type galaxies and right-hand panels show satellites of late-type galaxies. Top panels show satellites of primary galaxies more luminous than the median ($M_r - 5 \log h < -21.1$) while bottom panels show satellites of the less luminous primary galaxies ($M_r - 5 \log h > -21.1$). The vertical lines mark the maximum radial extent for satellites. These satellites are not included in the remaining plots. (d) Distribution of velocity differences between satellites and their primary. Panels are as in (c).

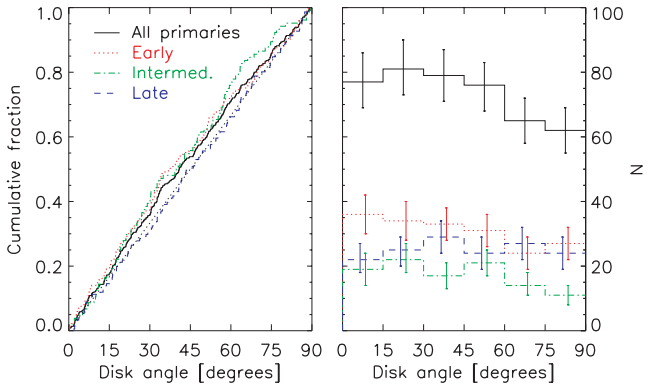

Figure 4. Left-hand panel: cumulative distribution of angle between the major axis of the primary and the location of the satellite ('disc angle'). The thick black/solid, red/dotted, green/dot–dashed and blue/dashed lines refer to the distribution of satellites around all primaries, early-, intermediate- and late-type primaries, respectively. The thin dotted line shows the distribution expected if satellites were isotropically distributed. Right-hand panel: differential distribution of the disc angles. The error bars are determined by bootstrap resampling of all primary galaxies.

around the early-type primaries if it were not physically present (see Appendix D).

Our measured alignment must be a lower limit on the intrinsic three-dimensional alignment for several reasons. First, images of triaxial elliptical galaxies contain isophotal twists due to projection effects, which introduce scatter between the isophotal PA we use and the intrinsic three-dimensional major axis. Secondly, galaxies seen closer to their symmetry axis have their anisotropic signal diluted. Finally, interlopers may dilute the signal.

In Fig. 5(a), we plot the mean disc angle of satellites as a function of projected separation from their primary. Satellites are binned in three annuli spaced evenly in radius from 35 to 500 h^{-1} kpc and are separated into those more luminous and less luminous than the median $M_r - 5 \log h = -21.1$. There is no significant trend with radius. Our intermediate-separation bin covers approximately the same radii as the outermost bin of AB07, in which they detect minor-axis alignment around late-type primaries; our mean disc angle around late-types at these radii is also greater than 45°, but not at a statistically significant level. While we do not detect the major-axis alignment that they see at small radii, a large number of systems in their innermost radial bin fall within the 35 h^{-1} kpc region that we exclude to avoid contamination from H II regions in the outskirts of the parent galaxy; if such regions are mistakenly included as satellites, they will bias the result towards major-axis alignment.

In Fig. 5(b), we compare the anisotropy as a function of the luminosity of the primary, luminosity of the satellite and the difference in magnitude between the primary and satellite. The widths of the bins are chosen such that there are similar numbers of satellites in each bin; in all panels, the symbols are plotted at the mean luminosity or mean ΔM_r of the galaxies in the bin. No clear trend

Table 5. Anisotropy of satellite and primary distributions.

Parameter	Full sample	Early-type primaries	Intermediate-type primaries	Late-type primaries
Disc angle				
KS probability	0.06	0.03	0.10	0.99
Mean disc angle [°]	42.5 ± 1.2	41.3 ± 0.9	40.5 ± 2.5	45.5 ± 2.1
Median disc angle [°]	$40.9^{+1.9}_{-1.6}$	$37.1^{+3.8}_{-3.5}$	$40.5^{+4.1}_{-7.8}$	$43.6^{+5.6}_{-2.1}$
Polar fraction	0.46 ± 0.02	0.44 ± 0.03	0.44 ± 0.05	0.50 ± 0.04
Early-type satellite mean	$42.5^{+4.5}_{-4.3}$	$36.6^{+6.0}_{-6.7}$	$49.5^{+6.6}_{-7.4}$	$47.7^{+11.7}_{-10.6}$
Intermediate-type satellite mean	$40.8^{+3.3}_{-3.7}$	$42.1^{+4.0}_{-4.5}$	$43.0^{+7.9}_{-7.6}$	$28.7^{+7.3}_{-6.9}$
Late-type satellite mean	42.8 ± 1.3	41.6 ± 2.3	$38.9^{+2.6}_{-2.8}$	46.2 ± 2.1
LSS angle				
KS probability	0.56	0.76	0.49	0.40
Mean LSS angle [°]	44.6 ± 1.2	$44.0^{+1.5}_{-1.7}$	$43.0^{+3.0}_{-3.2}$	46.4 ± 2.2
Disc/LSS angle				
With satellites – KS probability	0.06	0.4	0.05	0.10
– Mean	41.8 ± 1.4	43.4 ± 2.2	$39.8^{+2.5}_{-2.2}$	41.7 ± 2.3
All isolated – KS probability	0.0001	0.01	0.0006	0.17
– Mean	42.6 ± 0.7	42.1 ± 1.2	41.3 ± 1.2	43.6 ± 0.9

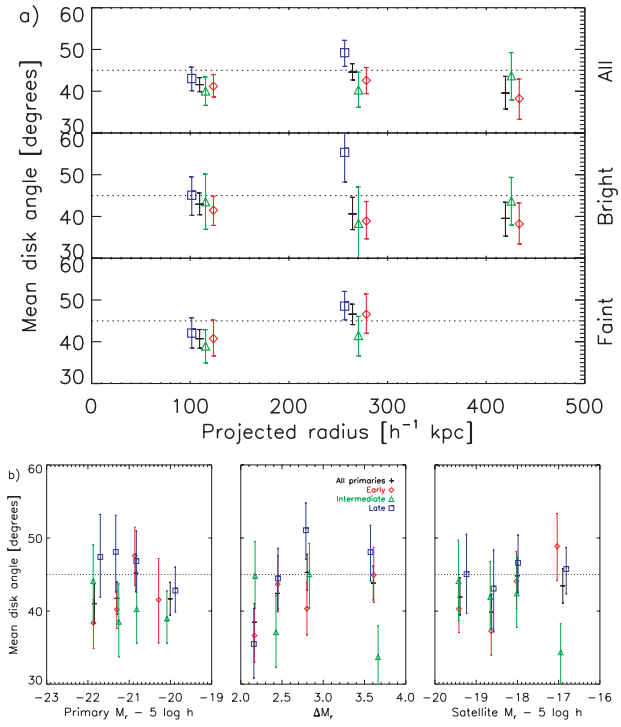

Figure 5. (a) Mean disc angle of satellites as a function of projected separation from their primary. Black pluses, red diamonds, green triangles and blue squares refer to satellites of all primaries, early-, intermediate- and late-type primaries, respectively. Radial bins are $155\,h^{-1}$ kpc wide and are plotted at the central bin radius with different symbols offset slightly for clarity. The top panel contains all satellites while the middle and bottom panels contain satellites of primaries with $M_r - 5\log h < -21.1$ and $M_r - 5\log h > -21.1$, respectively. (b) Mean disc angle of satellites as a function of the absolute magnitude of the primary (left-hand panel), the magnitude difference between the primary and satellite (middle panel) and the absolute magnitude of the satellite (right-hand panel). Bins are chosen to have approximately equal numbers of satellites per bin and plotted at the mean magnitude.

is apparent as a function of primary luminosity. The anisotropy shows a weak dependence on the magnitude difference between the primary and satellite, although the sense of the trend differs for different primary types. Around early-type primaries, those satellites that are not much fainter than their primaries show a stronger major-axis alignment than the satellites that are much fainter, while around intermediate-type primaries the opposite trend holds. Around late-type primaries, those satellites that are bright relative to their primary show $\sim 2\sigma$ major-axis alignment, while the faintest 50 per cent of the satellites relative to their primary do not (or, if anything, show a *polar* distribution, although not at a statistically significant level). These trends could either reflect a dependence on the degree to which the primary dominates, i.e. it could truly depend on the magnitude difference, or reflect a dependence on the luminosity of the satellite. The right-hand panel of Fig. 5(b) reveals that the anisotropy around intermediate-type galaxies can equally well be explained as being a function of satellite luminosity, while the angular distributions around early- and late-type primaries are not; therefore, for these galaxies, the trends seen in the middle panel truly reflect a dependence on the relative dominance of the primary.

Koch & Grebel (2006) found that only the early-type satellites of M31 have a polar alignment. Y06 and Faltenbacher et al. (2007) found that the red satellites of red primaries show stronger major-axis alignment than the blue satellites, and SL04 found that quiescent satellites show stronger anisotropy than star-forming satellites. To determine if these signals are evident in our sample, we split the sample by the galaxy type of both the primary and satellite, and plot the distributions in Fig. 6. Mean disc angles as a function of satellite type are given in rows 5 through 7 of Table 5. Although we see small deviations for particular subsamples (e.g. the early- versus late-type satellites of intermediate-type primaries, or the intermediate-type satellites of late-type primaries), none is statistically significant due to the small number of early- and intermediate-type satellites.

In Section 2.4, we excluded primary galaxies with isophotal axis ratios $b/a > 0.8$. Our choice of cut-off is motivated by Fig. 7, where we plot the mean disc angle around primaries with axis ratios less than or equal to the plotted abscissa. A cut-off at $b/a = 0.8$ provides enough systems that the results have converged, while avoiding the dilution in the signal seen at higher values of b/a. For a circular disc

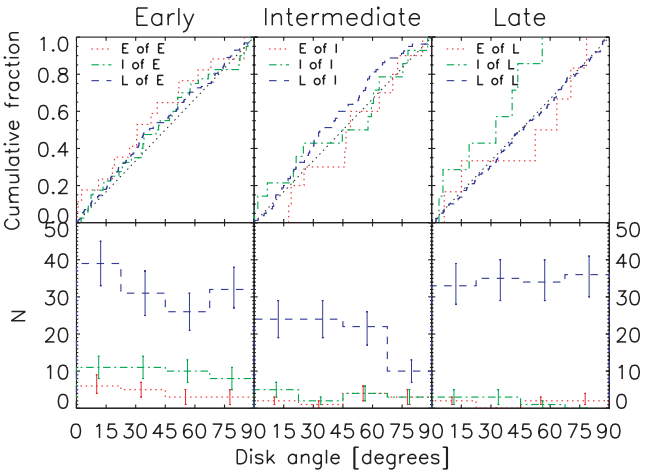

Figure 6. Cumulative (top panel) and differential (bottom panel) distributions of disc angle as a function of morphological type of both the primary and satellite. The three panels specify the type of the primary, while line colours and styles denote the type of the satellite.

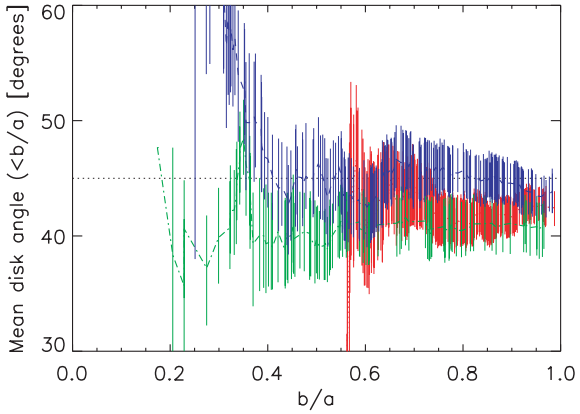

Figure 7. Mean disc angle for satellites of primaries with isophotal axis ratios less than or equal to the plotted abscissa. One error bar is plotted at the location of each primary galaxy. Colours/line styles are as in Fig. 4.

galaxy of intrinsic thickness 0.2, this corresponds to an inclination of 43°.

As discussed in Section 2.3.3, it is difficult to assess the effects of some of the selection parameters using the mock catalogues. Therefore, we now empirically investigate the effects of varying all of the selection parameters, including several parameters that have been neglected by many previous studies. In Fig. 8, we plot the mean disc angle and the sample size as we adjust $N_{\rm viol}$, $f_{\rm sat}$ and whether or not the survey magnitude limit or survey edge is taken into account. The mean disc angles are shown as symbols with error bars while the early- and late-type sample sizes are shown as histograms above and below (the intermediate-type sample sizes show identical trends).

In panel (a), we compare our combined NED and photometric redshift-based method of dealing with criteria violators, a method that only uses the photometric redshift, and methods based on a cut at various values of $N_{\rm viol}$. More restrictive values of $N_{\rm viol}$ lead to smaller sample sizes, particularly for $N_{\rm viol} \leq 4$. The measured anisotropy is relatively constant as a function of $N_{\rm viol}$. Our combined NED+photometric redshift method produces a sample size equivalent to using $N_{\rm viol} = 1$, and therefore recovers a reasonable fraction of the sample available from ignoring the presence of violators, while conservatively excluding any systems that could contaminate the sample. In panel (b), we plot the effects of $f_{\rm sat}$. The measured anisotropy rises as $f_{\rm sat}$ is reduced to very low values; this is accompanied by a sharp decrease in sample size. As indicated by Fig. 5(b), this indicates that in many cases the anisotropy is related to the dominance of the primary galaxy, and samples selected with large values of $f_{\rm sat}$ may be significantly contaminated. In panel (c), we show the effects of ignoring the survey magnitude limit or the survey edge. Both samples are marginally larger with no significant change in the measured anisotropy.

Although the exact strength of the anisotropy can vary with some of these oft-neglected parameters, the qualitative result that the satellites of early-type and possibly intermediate-type galaxies show a major-axis distribution while the satellites of late-type galaxies are isotropically distributed is not dependent on the value of any one of these parameters. Varying the other parameters from Table 1 has very little effect on the measured anisotropy, as anticipated by the results of B05, who found identical results in three samples with quite different values of these parameters.

3.2 Satellite and primary distribution relative to LSS

If satellites are accreted from filaments, then the most recently accreted satellites will be aligned preferentially with the surrounding filamentary LSS. We test this expectation by determining the axis of the LSS surrounding each primary galaxy. To determine this axis, we use all spectroscopic galaxies with projected radii between 1000 and 3000 h^{-1} kpc (thereby explicitly ensuring that there is no overlap between the galaxies used to determine the orientation of the LSS and those used to evaluate the isolation of the primary or the satellites themselves) with velocities that differ from that of the primary by no more than 400 km s^{-1}. The velocity dimension of this cylinder is significantly smaller than the cylinder used to select isolated galaxies and satellites. This is because filaments are not virialized structures and their intrinsic velocity dispersion about the Hubble flow is much lower than that inside a halo (for example, the scatter about the Hubble flow among the galaxies surrounding the Local Group is a mere 85 km s^{-1}, or as low as 40 km s^{-1} if galaxies inside virialized groups are excluded; Karachentsev et al. 2003), and therefore a much smaller additional velocity is required to account for peculiar velocities on top of the Hubble component of 300 km s^{-1} corresponding to the radial dimension of the cylinder. We calculate the PA and axial ratio of the distribution on the sky of these surrounding galaxies by diagonalizing the moment of inertia tensor relative to the primary galaxy. We have used the mock catalogues to confirm that this procedure reliably recovers the three-dimensional PA of the LSS surrounding the primary (see Appendix E).

Fig. 9 shows the distribution of angles between the PA of the great circle connecting the primary and the satellite and the PA of the LSS surrounding the primary ('LSS angles'; as with the disc angles, these are folded into the range 0°–90°). We present the results from KS tests and the mean LSS angles in Table 5.

The satellites of each population of galaxies are consistent with being isotropically distributed with respect to the LSS. However, all samples except that around late-type primaries have mean LSS angles less than 45°. Further data are required to determine if this hint of an alignment is real. In Fig. 10, we plot the mean LSS angle as a function of radial separation from the primary. Although each individual point is consistent with isotropy, the satellites at large

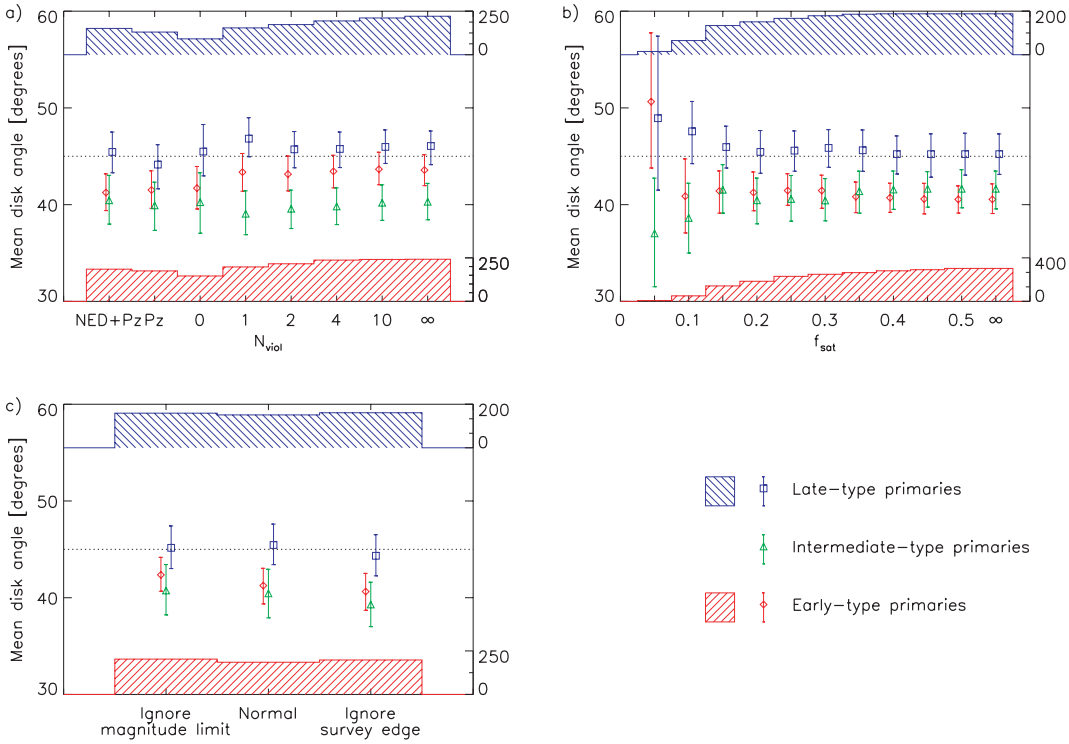

Figure 8. Effects of varying the selection parameters on the results and sample size. In each plot, the mean disc angle for early-/intermediate/late-type primaries is shown as the red diamond/green triangle/blue square symbols with error bars, while the sample size for the early- and late-type samples is shown as histograms below and above. The scale for each histogram is shown on the right-hand side of each plot. The histograms for the intermediate-type samples show identical trends. (a) The effects of replacing the fiducial NED plus photometric redshift ('NED + Pz') method for dealing with violators with either a pure photometric redshift method ('Pz') or a cut on $N_{\rm viol}$. (b) The effects of changing $f_{\rm sat}$. (c) The effects of limiting primaries to be at least $m_{\rm inner}$ magnitudes brighter than the survey limit and be at least projected radii $R_{\rm outer}$ from the edge of the photometric survey footprint and $R_{\rm sat}$ from the edge of the spectroscopic survey footprint.

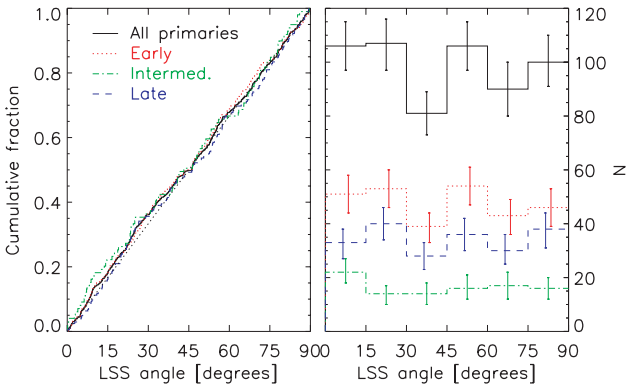

Figure 9. Left-hand panel: cumulative distribution of angle between the axis of the local LSS and the location of the satellite ('LSS angle'). The thick black solid/red dotted/green dot–dashed/blue dashed lines refer to the distribution of satellites around all primaries, early-, intermediate- and late-type primaries, respectively. The thin dotted line shows the distribution expected if satellites are isotropically distributed. Right-hand panel: differential distribution of the LSS angles. The error bars are determined by bootstrap resampling of all primary galaxies.

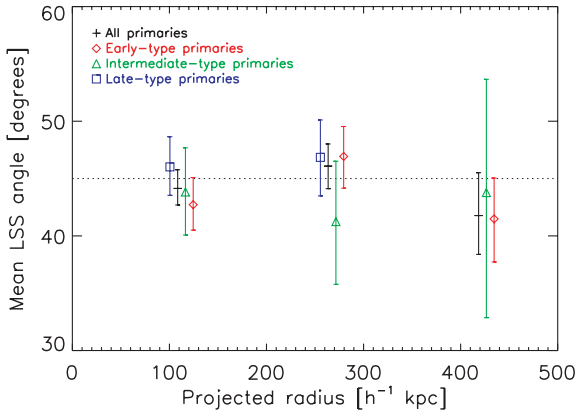

Figure 10. Mean LSS angle of satellites as a function of their projected separation from the primary. Black pluses, red diamonds, green triangles and blue squares refer to satellites of all primaries, early-, intermediate- and late-type primaries, respectively. Symbols are offset in radius slightly for clarity.

separations all have mean LSS angles less than 45° (as there are by definition no satellites of late-types in this bin, this may explain why the late-types also show no hint of LSS alignment.). Further information may be gained by plotting the LSS alignment as a function of satellite type (Figs 11 and 12). Although the number of early- and intermediate-type satellites is too small to draw any conclusions, the late-type satellites that are found at large radius are aligned with the LSS at the 2σ level.

Given the orientation of the primary galaxy and the LSS, we now investigate their relative alignment. The orientation of a disc galaxy is determined by its angular momentum, which originates from tidal

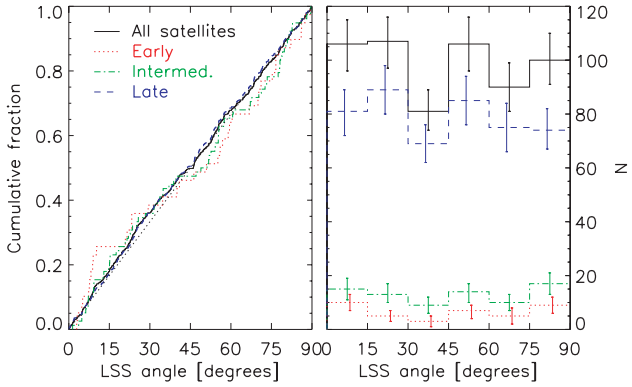

Figure 11. As in Fig. 9, but separated by the classification of the satellite galaxy.

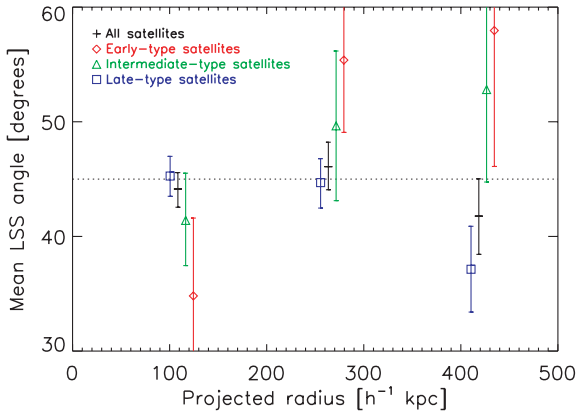

Figure 12. As in Fig. 10, but separated by the classification of the satellite galaxy.

torques due to the surrounding material. Analytic arguments and cosmological simulations suggest that this angular momentum (and therefore the disc spin axis) aligns with the intermediate axis of the surrounding mass distribution, and such alignment has been measured for disc galaxies in the supergalactic plane (Navarro, Abadi & Steinmetz 2004) and for galaxies in SDSS and 2dFGRS on the surfaces of voids (Trujillo, Carretero & Patiri 2006). The orientation of an early-type galaxy is determined by its anisotropic velocity ellipsoid, as is that of its halo; therefore, the two are expected to be aligned, and preferentially aligned with the LSS (Bailin & Steinmetz 2005). This has been measured for BCGs at low (Argyres et al. 1986; Lambas, Groth & Peebles 1988; Muriel & Lambas 1989) and high (Donoso, O'Mill & Lambas 2006) redshift, but not for field early-types. We directly compared the PA of our primary galaxies to that of their local LSS. For this comparison, we use all isolated galaxies that pass both the 'Disc' and 'LSS' quality cuts, regardless of whether they host satellite galaxies; our results are unchanged if we only include those that host satellite galaxies. The distributions are shown in Fig. 13, and the associated mean angles and KS test probabilities of being drawn from an isotropic distribution are given in Table 5. There is a detection of alignment between the orientation of isolated early-type galaxies and the surrounding LSS at 99 per cent confidence and strong alignment for isolated intermediate-type galaxies at 99.94 per cent confidence. We do not detect a significant alignment for isolated late-type galaxies. The

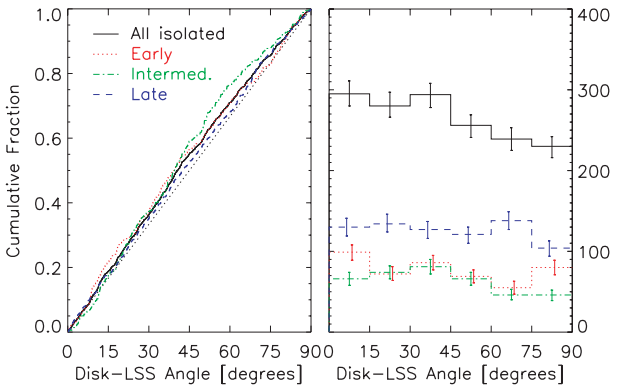

Figure 13. Cumulative (left-hand panel) and differential (right-hand panel) distributions of angles between the major axes of isolated galaxies and their surrounding LSS. The sample contains all isolated galaxies that pass the 'disc' and 'LSS' sample quality cuts, regardless of whether they host any satellite galaxies. Red/dotted lines refer to early-type galaxies while blue/dashed lines refer to late-type galaxies.

samples containing all isolated galaxies and only those with satellites are consistent with each other.

3.3 Satellites in the Local Group

Many satellites of the two dominant galaxies in the Local Group, the Milky Way and M31, appear to lie on planes that are highly inclined to their parent discs (Metz et al. 2007, and references therein). In order to determine how the anisotropy of the SDSS galaxies compares to the anisotropy around the Local Group spirals, we have determined the signal that we would have recovered around both the Milky Way and M31 if they had fallen into our sample.[6] Based on the distribution of primary and satellite magnitudes in our sample (Fig. 3a), we use all satellites with absolute magnitudes within 5 mag of their primary; for the Milky Way, this consists of the LMC and Small Magellanic Clouds (SMC), and for M31, this consists of M33, IC 10, M32 and NGC 205. The three-dimensional locations of these satellites with respect to their parent galactic disc are taken from Metz et al. (2007), using the McConnachie & Irwin (2006) parameters for the M31 satellites. We select 20 000 random viewing directions isotropically distributed about each galaxy and calculate the disc angle for each satellite from each viewing direction. We calculate the mean disc angle of the satellites averaged over all viewing angles where the projected axis ratio of the parent disc is less than 0.8 to provide a direct comparison to the SDSS sample.

The resulting anisotropies are listed in Table 6. The satellites of the Local Group spirals show polar distributions with mean disc angles of 49°.1 and 54°.0 for the satellites of the Milky Way and M31, respectively. We do not measure such a polar distribution around late-type disc galaxies in SDSS. However, we do measure a minor-axis alignment of this magnitude among those satellites much fainter than their primary (see Fig. 5b), and most of the Local Group satellites above meet that description. Therefore, perhaps the dependence of satellite anisotropy on the degree of primary

[6] In fact, neither the Milky Way nor M31 would fall into our sample if they were observed in a redshift survey because the presence of each would violate the isolation criteria around the other. Our isolation criteria are required to be so strict in order that systems intrinsically less isolated than Local Group galaxies are not mistakenly included.

Table 6. Anisotropy of Local Group satellites.

Parameter	Milky Way	M31
Mean disc angle [°]	49.1	54.0
Median disc angle [°]	47.7	53.4
Polar fraction	0.57	0.60

dominance may explain the discrepancy between the satellites of the Local Group spirals and the results from galaxy redshift surveys, or we are simply the victims of coincidence and small-number statistics.

4 COMPARISON WITH PREVIOUS RESULTS: THE EFFECTS OF ENVIRONMENT

Our results indicate that the satellites of isolated early-type galaxies show a preference for lying near the major axis of the primary, while those of intermediate-type galaxies may lie near the disc plane and those of late-type galaxies are isotropically distributed. The result of combining these populations gives a distribution that is purely a function of the morphological mixture in the sample of isolated galaxies; in our case, the early- and intermediate-type galaxies dominate over the late-type galaxies and therefore we find that satellites tend to exhibit a net major-axis alignment.

It is interesting to compare our results to those of previous studies. Our results for late-type galaxies agree with previous detections of an isotropic satellite distribution (SL04; AZPK; APPZ; Y06), and our results for early-type galaxies agree with previous detections of major-axis alignment (SL04; Y06; APPZ; AB07). Our intermediate-type galaxies would have been identified as part of the 'early'-type sample by those studies that used colour to classify galaxies, and would have been split between apparent ellipticals and apparent disc galaxies depending on inclination by those studies that classified galaxies by eye (see Bailin & Harris 2008b). As the anisotropy around intermediate- and early-type galaxies is similar, the former situation would not have affected the measured distribution, while in the latter case the relatively small number of contaminating intermediate-types would not have strongly affected the measured distribution around late-types. Finally, our results for the full sample agree with SL04, B05, Y06 and AB07, who all found that the full sample shows major-axis alignment.

The main disagreement between our results and the previous studies is with those studies that found a polar alignment of satellites around late-type galaxies (Holmberg 1969; ZSFW). However, there are physical subclasses of systems for which our results are consistent with a polar alignment (i.e. although our results in these regimes are consistent with isotropy, and we therefore do not claim detection of a polar alignment, the mean disc angles are sufficiently larger than 45° that they are also consistent with a polar alignment): satellites at intermediate separation from their primary, and those that are much fainter than their primary. The polar alignment found by these studies may be explained if they were dominated by such satellites; indeed, ZSFW detected their polar alignment for satellites with similar projected separations as our intermediate separation bin, and dominance by relatively faint satellites may explain the alignment seen around the Milky Way and M31 (see Section 3.3).

To determine the effects of different selection criteria on the measured anisotropy, we adopt the criteria from the previous studies (as given in Table 1) to select corresponding samples of galaxies from SDSS DR6 and to measure the disc angle distribution. The mean value of the disc angle determined by the previous studies and the value we derive using identical selection criteria are shown in Fig. 14 as a function of $f_{\rm non-dom}$, the fraction of satellites estimated to lie around non-isolated primaries according to the mock catalogue analysis (see Table 3). For simplicity, in this figure only we separate galaxies into two classes, using the location on the CMD. More details about the comparison are presented in Appendix F. This figure confirms that if we select galaxies according to the criteria used in each previous study, we recover their results.

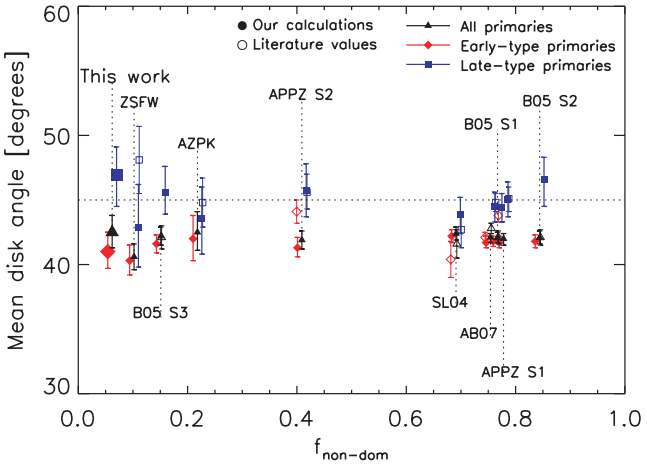

Figure 14. Mean disc angle of satellites selected using each set of criteria versus $f_{\rm non-dom}$, the fraction of satellites selected using each criteria that lie around non-isolated primaries (see Table 3). Colours/symbols are as in Fig. 5, where we have used location on the CMD to separate early- from late-type galaxies in all cases. Filled symbols with thick error bars indicate our calculations, while open symbols with thin error bars indicate the values given in each previous study. As the degree of agreement is excellent, the filled and open symbols typically lie almost overtop of each other. Early- and late-type symbols are offset in $f_{\rm non-dom}$ for clarity.

The angular distribution found using each sample is quite similar. However, the selected galaxies lie in very different environments. Our selection criteria have been fine-tuned using mock catalogues to select satellites of isolated primaries. While most previous authors have also implemented selection criteria aimed at identifying isolated primaries, the results of Section 2.3 indicate that they have had variable success. In particular, the fraction of satellites around non-isolated primaries is over 50 per cent in several of the previous studies. The satellites in these systems should be considered group members rather than satellites of isolated galaxies, as should those of Y06, Faltenbacher et al. (2007) and Wang et al. (2008), whose selection criteria were tuned to find associated galaxies with no constraints on whether the largest galaxy in each group is isolated.

The combination of our results and those of previous studies constrains the environmental dependence (or lack thereof) of the satellite distribution. Satellites surrounding spheroidal galaxies show the same major-axis alignment regardless of whether that spheroid is isolated or at the centre of a group. Similarly, the satellites surrounding isolated late-type galaxies are as isotropically distributed as the members of groups that surround late-type galaxies. Although previous studies have not identified intermediate-type galaxies, we can select galaxies using their criteria and examine the distribution of those satellites around intermediate-type galaxies. For example, when using the sample generated by the B05 S2 criteria, which lies at the far right-hand side of Fig. 14 and contains almost

85 per cent group members, the satellites of intermediate-type galaxies have a mean disc angle of $41.^{\circ}5 \pm 0.^{\circ}9$, in good agreement with the planar alignment tentatively detected around isolated intermediate-type galaxies using our fiducial criteria. Therefore, we conclude that group-specific processes are not responsible for the angular distributions of their member galaxies, but rather processes that also apply to the satellites of isolated galaxies.

5 SUMMARY AND DISCUSSION

We summarize our results as follows.

(i) Satellites of isolated early-type spheroidal galaxies lie preferentially along the major axis of the galaxy. The degree of alignment increases slightly for satellites that are brighter relative to their primary.

(ii) Satellites of isolated disc galaxies appear to have different angular distributions depending on the colour of the disc. Satellites of *red* discs (intermediate-type galaxies) show hints of lying preferentially near the disc plane, with intrinsically or relatively fainter satellites showing a tendency to stronger anisotropy. Satellites of *blue* discs (late-type galaxies) are distributed isotropically.

(iii) Late-type satellites that are found far from their primary show preferential alignment with the surrounding LSS (i.e. filaments) (Fig. 12).

(iv) Isolated early- and intermediate-type galaxies show an alignment with the surrounding LSS. This alignment is strongest for intermediate-type galaxies (with a KS test significance of 99.94 per cent).

(v) The angular distribution of group members about the BGG is very similar to the distribution of satellites around an isolated galaxy of the same type.

(vi) Great care must be taken in order to select truly isolated galaxies and their satellites in galaxy redshift surveys. Unless the region immediately surrounding the primary is devoid of galaxies too large to be considered satellites (*whether or not those galaxies have been observed spectroscopically*), the sample will be dominated by group members rather than isolated galaxies.

These results provide us with the foundations on which we can build our understanding of the mass distribution in and around galaxies and raise a number of interesting questions. What can we learn about the role of dynamical effects in driving preferential alignments of satellites? What is the nature of these effects and does it depend on the morphological type and history of the galaxy? What role is played by the host dark matter halo? What role is played by the larger scale environment? Our results allow us to begin to address these questions.

The most straightforward interpretation of the preferential alignment of satellites at large projected radii with the surrounding LSS is that this is a signature of the anisotropic infall of satellite galaxies along filaments. This interpretation is favoured by the following observations.

(i) The mean angle between the projected positions of satellites and the surrounding LSS (i.e. the LSS angle) is similar around different types of galaxies.

(ii) The alignment is present for *only* the more recently accreted satellites, i.e. those that are most distant and those blue late-type satellites for which halo-specific transformation mechanisms have not yet had time to operate.

(iii) The alignment is distinctive when compared to the alignment of the satellites with respect to their primary.

This evidence argues in favour of an origin that is imposed by the larger scale environment rather than one driven by the primary galaxy. In other words, it is improbable that the dynamics of the most recently accreted satellites will be significantly affected by any process internal to the primary's dark matter halo. This is in agreement with the results of cosmological simulations (Knebe et al. 2004; Libeskind et al. 2005; Zentner et al. 2005).

The relationship between the orientation of a galaxy and its surrounding LSS can be understood in terms of the relationship between the orientation of the galaxy's dark matter halo and its surrounding LSS *and* the galaxy's orientation within its dark matter halo. Cosmological *N*-body simulations predict that dark matter haloes are strongly triaxial systems in the absence of baryons (e.g. Allgood et al. 2006), and these haloes tend to align with their major axes along the large-scale filaments and their minor axes perpendicular to filaments (Bailin & Steinmetz 2005).

However, the presence of baryons can have a dramatic effect on the shapes and internal alignments of dark matter haloes with interesting consequences for the haloes of disc galaxies. A number of studies have shown that cooling baryons at the centre of a dark matter halo tend to circularize the orbits of dark matter particles, modifying the halo's inner mass profile (e.g. Gustafsson, Fairbairn & Sommer-Larsen 2006) and reducing the ellipticity of the halo's isodensity surfaces (e.g. Dubinski 1994; Kazantzidis et al. 2004). Bailin et al. (2005) examined the structure of the host haloes of several disc galaxies that formed in high-resolution cosmological *N*-body hydrodynamical simulations, and discovered that haloes consisted of two distinct regions. The inner halo is flattened along the disc axis, while the orientation of the outer halo is unrelated to that of the inner halo and is unaffected by the presence of the luminous galaxy.

The Bailin et al. (2005) result is interesting because it implies that the major axis of the inner halo around a typical disc galaxy is aligned with the major axis of the light distribution, while the major axis in the outer region is independent of the light but is aligned with the LSS. If satellite galaxies are more common along the halo major axis, then this 'twisting' of the halo should be evident in the distribution of satellites around disc galaxies. Indeed, we observe that the outermost satellites around all types of galaxies are preferentially aligned with the LSS, while the inner satellites around intermediate-type disc galaxies [which correspond most closely to the relatively red-concentrated simulated discs studied by Bailin et al. (2005)] are found preferentially in the disc plane. However, the significant relative alignment between intermediate-type galaxies and the LSS argues that some residual halo–LSS alignment remains.

In the case of early-type galaxies, the orientation of the galaxy with respect to its dark matter halo has not been studied explicitly in a cosmological context. However, we would expect that the shapes of both their stellar and dark matter components are supported by their anisotropic velocity ellipsoid. Consequently, we would expect that both the galaxy and its dark matter halo will share the same orientation, and therefore the galaxy will tend to align with the surrounding LSS (Bailin & Steinmetz 2005), as is observed.

How should we interpret the preferential alignments of satellites around isolated galaxies? Can we determine whether the alignments are imprinted by the dynamical effects of the galaxy or the host dark matter halo?

Agustsson & Brainerd (2006), AB07 and Kang et al. (2007) studied the angular distribution of satellite galaxies in cosmological simulations selected according to the criteria of B05, AB07 and Y06, respectively (note that all of these criteria select samples dominated by groups). The orientation of a mock galaxy must be assumed and

so these authors explored different assumptions about how primary galaxies are oriented with respect to their dark matter haloes and the larger scale environment. They found that if the primary galaxy is a spheroid whose principal axes are perfectly aligned with those of its dark matter halo, then satellites in these systems tend to show a major-axis anisotropy that is stronger than observed in the groups whose BGG is an early-type galaxy. However, if there is a small offset between the principal axes of the galaxy and its halo, as may arise if the galaxy aligns with the halo's angular momentum rather than its minor axis, then the anisotropy is of the same order that is observed. Because the alignment of satellites relative to isolated early-types is identical to that seen in galaxy groups whose BGG is an early-type, we may therefore conclude that the principal axes of isolated early-types are similarly well aligned with those of their dark matter haloes ($\sim 20^\circ$). As we argued above, this is in accordance with our expectation that the dynamics of baryons and dark matter in collisionless ellipsoidal systems are similar.

The theoretical situation around discs is less clear. If the disc is oriented perpendicular to its halo's angular momentum, it is simply a special case of an oblate spheroid, and therefore these studies predict that its satellites will exhibit major-axis alignment. This is consistent with what we observe around red discs, but in stark contrast to what is seen around blue discs. If, on the other hand, the angular momenta of galaxy discs align with the intermediate axis of the surrounding mass distribution, as seen in the simulations of Navarro et al. (2004), then satellites in these systems show no preferential alignments, as we observe around blue discs. If we interpret disc colour as a measure of how long the baryonic material has been a part of the luminous galaxy, then perhaps red discs have had more time to come to equilibrium with their halo, while most of the material in blue discs has been acquired more recently and retains a memory of the external tidal torques.

However, these explanations are still largely speculative. A theoretical analysis that takes into account the detailed dependencies of the satellite distribution, the alignment of satellites with the LSS and the differences between early-type spheroidal galaxies, intermediate-type red disc galaxies and late-type blue disc galaxies must be performed to determine whether the distribution of satellites is determined predominantly by the orientation of the halo or if dynamical processes within the halo are important. We are in the process of performing such an analysis (Power et al., in preparation).

ACKNOWLEDGMENTS

JB thanks Mike Blanton for writing KCORRECT; the SDSS help desk for their help with the Catalog Archive Server; Stéphane Herbert-Fort, Pavel Kroupa and Manuel Metz for useful discussions; and John and Lexi Moustakas for writing the RED IDL cosmological routines. Early stages of this research benefited from three-dimensional visualization conducted with the S2PLOT programming library (Barnes et al. 2006).

JB acknowledges the financial assistance of the Australian Research Council. CP and BKG gratefully acknowledge the support of the Australian Research Council supported 'Commonwealth Cosmology Initiative', DP 0665574. During the course of this work, PN acknowledges funding from a Zwicky Fellowship at ETH and a PPARC PDRA Fellowship at the IfA. DZ acknowledges support from NASA LTSA award NNG5-GE82G, NSF grant AST-0307482 and a Guggenheim fellowship. The authors also thank the NYU Physics department and Centre for Cosmology and Particle Physics for their generous support during his sabbatical there.

Funding for the SDSS and SDSS II has been provided by the Alfred P. Sloan Foundation, the participating institutions, the National Science Foundation, the US Department of Energy, the National Aeronautics and Space Administration, the Japanese Monbukagakusho, the Max Planck Society and the Higher Education Funding Council for England. The SDSS Web site is http://www.sdss.org/.

The SDSS is managed by the Astrophysical Research Consortium for the participating institutions. The participating institutions are the American Museum of Natural History, Astrophysical Institute Potsdam, University of Basel, University of Cambridge, Case Western Reserve University, University of Chicago, Drexel University, Fermilab, the Institute for Advanced Study, the Japan Participation Group, Johns Hopkins University, the Joint Institute for Nuclear Astrophysics, the Kavli Institute for Particle Astrophysics and Cosmology, the Korean Scientist Group, the Chinese Academy of Sciences (LAMOST), Los Alamos National Laboratory, the Max-Planck-Institute for Astronomy (MPIA), the Max Planck Institute for Astrophysics (MPA), New Mexico State University, Ohio State University, University of Pittsburgh, University of Portsmouth, Princeton University, the United States Naval Observatory and the University of Washington.

This research has made use of the NED which is operated by the Jet Propulsion Laboratory, California Institute of Technology, under contract with the National Aeronautics and Space Administration.

REFERENCES

Adelman-McCarthy J. K. et al., 2008, ApJS, 175, 297
Agustsson I., Brainerd T. G., 2006, ApJ, 650, 550 (AB06)
Agustsson I., Brainerd, T. G. 2007, ApJ, submitted (arXiv:0704.3441) (AB07)
Allgood B., Flores R. A., Primack J. R., Kravtsov A. V., Wechsler R. H., Faltenbacher A., Bullock J. S., 2006, MNRAS, 367, 1781
Argyres P. C., Groth E. J., Peebles P. J. E., Struble M. F., 1986, AJ, 91, 471
Azzaro M., Zentner A. R., Prada F., Klypin A. A., 2006, ApJ, 645, 228 (AZPK)
Azzaro M., Patiri S. G., Prada F., Zentner A. R., 2007, MNRAS, 376, L43 (APPZ)
Bailin J., Steinmetz M., 2005, ApJ, 627, 647
Bailin J., Harris W. E., 2008a, MNRAS, 385, 1835
Bailin J., Harris W. E., 2008b, ApJ, 681, 225
Bailin J. et al., 2005, ApJ, 627, L17
Barnes D. G., Fluke C. J., Bourke P. D., Parry O. T., 2006, Publ. Astron. Soc. Aust., 23, 82
Basilakos S., Plionis M., Kovač K., Voglis N., 2007, MNRAS, 378, 301
Berlind A. A., Weinberg D. H., 2002, ApJ, 575, 587
Binggeli B., 1982, A&A, 107, 338
Blanton M. R. et al., 2003, AJ, 125, 2348
Brainerd T. G., 2005, ApJ, 628, L101 (B05)
Buote D. A., Jeltema T. E., Canizares C. R., Garmire G. P., 2002, ApJ, 577, 183
Chen J., Kravtsov A. V., Prada F., Sheldon E. S., Klypin A. A., Blanton M. R., Brinkmann J., Thakar A. R., 2006, ApJ, 647, 86
Cole S., Lacey C. G., Baugh C. M., Frenk C. S., 2000, MNRAS, 319, 168
Colless M. et al., 2001, MNRAS, 328, 1039
Conroy C., Wechsler R. H., Kravtsov A. V., 2006, ApJ, 647, 201
Conroy C. et al., 2007, ApJ, 654, 153
de Vaucouleurs G., de Vaucouleurs A., Corwin H. G., Buta R. J., Paturel G., Fouque P., 1991, Third Reference Catalogue of Bright Galaxies. Volume 1–3. Springer-Verlag, Berlin, (RC3)
Donoso E., O'Mill A., Lambas D. G., 2006, MNRAS, 369, 479
Dubinski J., 1994, ApJ, 431, 617
Eke V. R. et al., 2004, MNRAS, 355, 769
Eisenstein D. J. et al., 2001, AJ, 122, 2267

Faltenbacher A., Li C., Mao S., van den Bosch F. C., Yang X., Jing Y. P., Pasquali A., Mo H. J., 2007, ApJ, 662, L71
Fellhauer M. et al., 2006, ApJ, 651, 167
Gao L., White S. D. M., Jenkins A., Stoehr F., Springel V., 2004, MNRAS, 355, 819
Gustafsson M., Fairbairn M., Sommer-Larsen J., 2006, Phys. Rev., 74, 123522
Hartwick F. D. A., 2000, AJ, 119, 2248
Helmi A., 2004, ApJ, 610, L97
Herbert-Fort S., Zaritsky D., Jin Kim Y., Bailin J., Taylor J. E., 2008, MNRAS, 384, 803
Hoekstra H., Yee H. K. C., Gladders M. D., 2004, ApJ, 606, 67
Holmberg E., 1969, Ark. Astron., 5, 305
Ibata R., Lewis G. F., Irwin M., Totten E., Quinn T., 2001, ApJ, 551, 294
Jenkins A., Frenk C. S., White S. D. M., Colberg J. M., Cole S., Evrard A. E., Couchman H. M. P., Yoshida N., 2001, MNRAS, 321, 372
Johnston K. V., Law D. R., Majewski S. R., 2005, ApJ, 619, 800
Kang X., van den Bosch F. C., Yang X., Mao S., Mo H. J., Li C., Jing Y. P., 2007, MNRAS, 378, 1531
Karachentsev I. D. et al., 2003, A&A, 398, 479
Kazantzidis S., Kravtsov A. V., Zentner A. R., Allgood B., Nagai D., Moore B., 2004, ApJ, 611, L73
Knebe A., Gill S. P. D., Gibson B. K., Lewis G. F., Ibata R. A., Dopita M. A., 2004, ApJ, 603, 7
Koch A., Grebel E. K., 2006, AJ, 131, 1405
Kroupa P., Theis C., Boily C. M., 2005, A&A, 431, 517
Lambas D. G., Groth E. J., Peebles P. J. E., 1988, AJ, 95, 996
Law D. R., Johnston K. V., Majewski S. R., 2005, ApJ, 619, 807
Libeskind N. I., Frenk C. S., Cole S., Helly J. C., Jenkins A., Navarro J. F., Power C., 2005, MNRAS, 363, 146
Libeskind N. I., Cole S., Frenk C. S., Okamoto T., Jenkins A., 2007, MNRAS, 374, 16
Liske J., Lemon D. J., Driver S. P., Cross N. J. G., Couch W. J., 2003, MNRAS, 344, 307
Lukić Z., Heitmann K., Habib S., Bashinsky S., Ricker P. M., 2007, ApJ, 671, 1160
Lynden-Bell D., 1976, MNRAS, 174, 695
Mandelbaum R. et al., 2005, MNRAS, 361, 1287
Mandelbaum R., Hirata C. M., Broderick T., Seljak U., Brinkmann J., 2006, MNRAS, 370, 1008
Martínez-Delgado D., Gómez-Flechoso M. Á., Aparicio A., Carrera R., 2004, ApJ, 601, 242
McConnachie A. W., Irwin M. J., 2006, MNRAS, 365, 902
Metz M., Kroupa P., Jerjen H., 2007, MNRAS, 374, 1125
Meyer M. J., Zwaan M. A., Webster R. L., Brown M. J. I., Staveley-Smith L., 2007, ApJ, 654, 702
Muriel H., Lambas D. G., 1989, AJ, 98, 1995
Navarro J. F., Abadi M. G., Steinmetz M., 2004, ApJ, 613, L41
Norberg P. et al., 2002, MNRAS, 332, 827
Norberg P., Frenk C. S., Cole S., 2008, MNRAS, 383, 646
Oyaizu H., Lima M., Cunha C. E., Lin H., Frieman J., Sheldon E. S., 2008, ApJ, 674, 768
Palma C., Majewski S. R., Johnston K. V., 2002, ApJ, 564, 736
Peñarrubia J., Kroupa P., Boily C. M., 2002, MNRAS, 333, 779
Power C., 2003, PhD thesis, Durham University
Prada F. et al., 2003, ApJ, 598, 260
Sales L., Lambas D. G., 2004, MNRAS, 348, 1236 (SL04)
Schechter P., 1976, ApJ, 203, 297
Schlegel D. J., Finkbeiner D. P., Davis M., 1998, ApJ, 500, 525
Seljak U., Zaldarriaga M., 1996, ApJ, 469, 437
Sheth R. K., Tormen G., 1999, MNRAS, 308, 119
Strauss M. A. et al., 2002, AJ, 124, 1810
Trujillo I., Carretero C., Patiri S. G., 2006, ApJ, 640, L111
van den Bosch F. C., Yang X., Mo H. J., 2003, MNRAS, 340, 771
van den Bosch F. C., Norberg P., Mo H. J., Yang X., 2004, MNRAS, 352, 1302
van den Bosch F. C., Yang X., Mo H. J., Norberg P., 2005, MNRAS, 356, 1233
Wang Y., Yang X., Mo H. J., Li C., van den Bosch F. C., Fan Z., Chen X., 2008, MNRAS, 385, 1511
West M. J., 1989, ApJ, 347, 610
Yang X., Mo H. J., van den Bosch F. C., 2003, MNRAS, 339, 1057
Yang X., Mo H. J., Jing Y. P., van den Bosch F. C., Chu Y., 2004, MNRAS, 350, 1153 (Y04)
Yang X., van den Bosch F. C., Mo H. J., Mao S., Kang X., Weinmann S. M., Guo Y., Jing Y. P., 2006, MNRAS, 369, 1293 (Y06)
York D. G. et al., 2000, AJ, 120, 1579
Zaritsky D., Smith R., Frenk C., White S. D. M., 1997a, ApJ, 478, 39
Zaritsky D., Smith R., Frenk C. S., White S. D. M., 1997b, ApJ, 478, L53 (ZSFW)
Zentner A. R., Kravtsov A. V., Gnedin O. Y., Klypin A. A., 2005, ApJ, 629, 219

APPENDIX A: THE CLF – PARAMETERS

Yang et al. (2003) deduced a functional form for the variation of the mass-to-light ratio with dark matter halo mass by comparing the Sheth & Tormen (1999) dark matter halo mass function with the Schechter luminosity function (Schechter 1976). They noted that the mass-to-light ratio must increase (decrease) with decreasing (increasing) halo mass, and proposed a parametrization for the variation of the average total mass-to-light ratio with halo mass

$$\frac{\langle M\rangle}{\langle L\rangle}(M) = \frac{1}{2}\left(\frac{M}{L}\right)_0 \left[\left(\frac{M}{M_1}\right)^{-\gamma_1} + \left(\frac{M}{M_1}\right)^{\gamma_2}\right]. \tag{A1}$$

Here, the free parameters correspond to M_1, the characteristic mass for which the mass-to-light ratio in b_J is equal to $(M/L)_0$, and γ_1 and γ_2 which determine the behaviour at the low- and high-mass ends of the mass function, respectively. We follow Y04 in adopting $M_1 = 10^{10.94}\,h^{-1}\,\mathrm{M}_\odot$, $(M/L)_0 = 124\,h\,(\mathrm{M/L})_\odot$ in b_J, $\gamma_1 = 2.02$ and $\gamma_2 = 0.30$.

The characteristic luminosity $\tilde{L}^*$ is parametrized in a similar manner:

$$\frac{M}{\tilde{L}^*} = \frac{1}{2}\left(\frac{M}{L}\right)_0 f(\tilde{\alpha}) \left[\left(\frac{M}{M_1}\right)^{-\gamma_1} + \left(\frac{M}{M_2}\right)^{\gamma_3}\right], \tag{A2}$$

where M_2 is a characteristic mass and γ_3 determines the behaviour at the high-mass end of the mass function; $\tilde{\alpha}$ follows

$$\tilde{\alpha} = \alpha_{15} + \eta \log(M_{15}), \tag{A3}$$

where M_{15} is the mass of the halo in units of $10^{15}\,h^{-1}\,\mathrm{M}_\odot$ and α_{15} and η are free parameters. We follow Y04 in adopting $M_2 = 10^{12.04}\,h^{-1}\,\mathrm{M}_\odot$, $\gamma_3 = 0.72, \eta = -0.22$ and $\alpha_{15} = -1.1$.

Expressions (A1) and (A2) allow an expression for $\langle L\rangle/\langle M\rangle$ to be derived, from which $\tilde{\Phi}^*$ is deduced;

$$\frac{\langle L\rangle}{\langle M\rangle}(M) = \int_0^\infty \Phi(L|M)\frac{L}{M}\,\mathrm{d}L = \Phi^*\frac{\tilde{L}^*}{M}\Gamma(\tilde{\alpha}+2) \tag{A4}$$

leads to

$$\tilde{\Phi}^*(M) = \frac{1}{\Gamma(\tilde{\alpha}+1,1)}\frac{\left[(M/M_1)^{-\gamma_1} + (M/M_2)^{\gamma_3}\right]}{\left[(M/M_1)^{-\gamma_1} + (M/M_1)^{\gamma_2}\right]}. \tag{A5}$$

Here, $\Gamma(x)$ and $\Gamma(x, a)$ are the Gamma and Incomplete Gamma functions, respectively; formally these are expressed as

$$\Gamma(x) = \int_0^\infty t^{x-1}\exp(-t)\,\mathrm{d}t \tag{A6}$$

and

$$\Gamma(x,a) = \int_a^\infty t^{x-1}\exp(-t)\,\mathrm{d}t. \tag{A7}$$

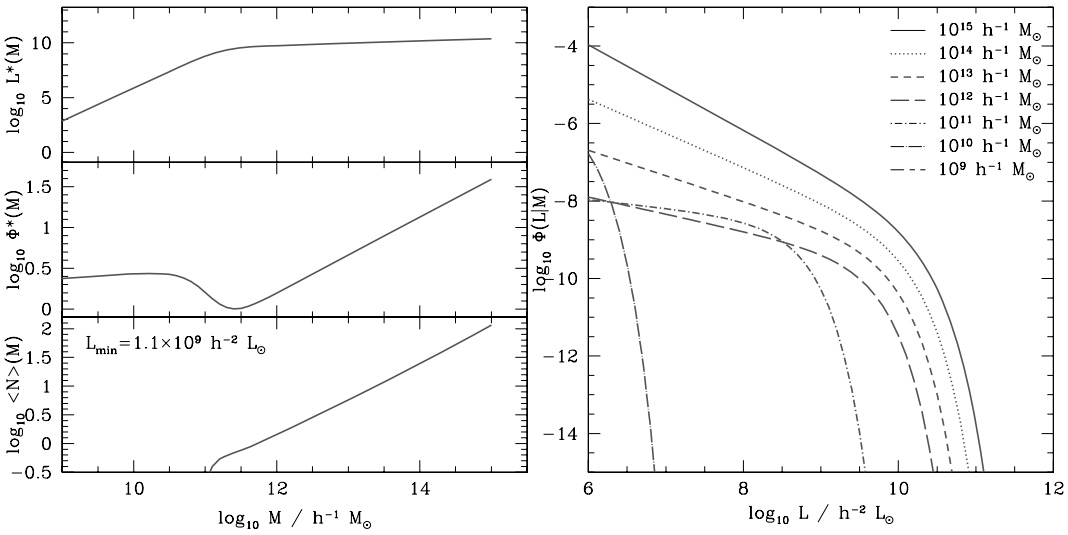

Figure A1. Left-hand panel: variation of the CLF parameters $\tilde{L}^*$ (upper panel) and $\tilde{\Phi}^*$ (middle panel), and the halo occupation number $\langle N\rangle\,(M)$ (bottom panel) with halo mass. We adopt the Y04 choice of 2dFGRS parameters and a minimum luminosity $L_{\rm min} = 1.1 \times 10^9\,h^{-2}\,{\rm L}_\odot$. Right-hand panel: Variation of the CLF with luminosity at fixed halo masses, for the Y04 parameters.

We note that Y04 denote the average mass-to-light ratio by $\langle M/L\rangle$ (see their equation 2). We prefer $\langle M\rangle/\langle L\rangle$ because the meaning is clear – the average luminosity associated with a halo of mass M is $\langle L\rangle$ and so the average mass-to-light ratio is $\langle M\rangle/\langle L\rangle$. If we adopt $\langle M/L\rangle$, this means that

$$\left\langle \frac{M}{L} \right\rangle (M) = \int_0^\infty \Phi(L|M)\frac{M}{L}\,{\rm d}L = \Phi^* \frac{M}{\tilde{L}^*}\Gamma(\tilde{\alpha}). \qquad \text{(A8)}$$

This produces an expression for $\tilde{\Phi}^*$ that is quite different from equation (A5), and which does not recover the correct behaviour of quantities such as $\langle N\rangle\,(M)$.

Having deduced the form of $\tilde{\Phi}^*$, we can compute the 'CLF' $\Phi(L|M)$,

$$\Phi(L|M){\rm d}L = \frac{\tilde{\Phi}^*}{\tilde{L}^*}\left(\frac{L}{\tilde{L}^*}\right)^{\tilde{\alpha}} \exp(-L/\tilde{L}^*){\rm d}L.$$

The upper left-hand panels of Fig. A1 show how $\tilde{L}^*$ and $\tilde{\Phi}^*$ vary with halo mass, while the right-hand panel shows the variation of $\Phi(L|M)$ with luminosity at a fixed halo mass for the Y04 choice of 2dFGRS parameters.

APPENDIX B: POPULATING DARK MATTER HALOES WITH GALAXIES – DETAILS

We perform a suite of cosmological N-body simulations and constructed catalogues of dark matter haloes at $z = 0$. Dark matter haloes are identified using a FOF algorithm with a linking length of $b = 0.2$ times the mean interparticle separation. For each of the groups identified in this way, we compute the virial mass M_{180}, defined as the mass of the spherical overdensity that is 180 times the critical density of the universe at $z = 0$. In the following discussion, we define a halo's mass M to be its virial mass M_{180} rather than $M_{\rm FOF}$, the mass of the FOF group; this is required by the Y04 prescription.

The minimum halo mass $M_{\rm min}$ that is 'reliably' recovered in each of the simulations governs the minimum luminosity, $L_{\rm min}$, that is used in constructing the mock catalogues. $L_{\rm min}$ defines the threshold luminosity fainter than which there are no galaxies. $M_{\rm min}$ is the halo mass above which we expect the mass function to be unaffected by finite numerical resolution; below this threshold the number density of haloes tends to be suppressed relative to the number density they would have in the limit of infinite numerical resolution. Previous studies have examined how the mass function is affected by finite mass and force resolution, time-stepping accuracy and starting redshift, as well as the influence of the group-finding algorithm used to identify dark matter haloes (e.g. Jenkins et al. 2001; Lukić et al. 2007). Jenkins et al. (2001) performed careful convergence tests and found that mass functions constructed from FOF groups are adversely affected by numerical effects below a halo mass equivalent to ∼20 particles. In this work, we adopt a more conservative lower mass limit of 50 particles to ensure that the mass function of haloes in higher density regions is converged (see chapter 3 of Power 2003); this gives $M_{\rm min} = 50\,m_{\rm part}$ in Table 2.

Having determined $M_{\rm min}$, we estimate $L_{\rm min}$ using the 'conditional probability distribution' $P(M|L)$ (see right-hand panel of Fig. 1, Y04). $L_{\rm min}$ is a critical parameter because it fixes the halo occupation number, the average number of galaxies per halo of mass M,

$$\langle N\rangle(M) = \tilde{\Phi}^*\Gamma(\tilde{\alpha}+1, L_{\rm min}/\tilde{L}^*). \qquad \text{(B1)}$$

The variation of $\langle N\rangle\,(M)$ with halo mass for the Y04 2dFGRS parameters and $L_{\rm min} = 1.1 \times 10^9\,h^{-2}\,{\rm L}_\odot$ is shown in the bottom left-hand panel of Fig. A1. This $L_{\rm min}$ is appropriate for the $M_{\rm min}$ in the mock catalogues A to E.

Note the important role played by the ratio $L_{\rm min}/\tilde{L}^*$ in equation (B1), which controls the number of galaxies per halo. At fixed $L_{\rm min}$, it increases dramatically as halo mass decreases, leading to low-mass haloes containing one 'central' galaxy at most, and as $L_{\rm min}$ decreases, the number of galaxies per halo increases. The number of galaxies per halo of mass M is Poisson distributed with a mean of $\langle N\rangle\,(M)$.

We also note that Yang et al. (2003) introduced a 'hard' lower mass cut-off of $M_{\rm min} = 10^9\,h^{-1}\,{\rm M}_\odot$ below which haloes cannot host galaxies – galaxy formation is suppressed in these haloes following cosmological reionization.

Having determined the number of galaxies hosted by a halo, we must assign luminosities. We follow Y04 and give special status to the central galaxy by assuming that it is the brightest in the halo

with an average luminosity

$$\langle L_c \rangle = \tilde{\Phi}^* \tilde{L}^* \Gamma(\tilde{\alpha}+2, L_1/\tilde{L}^*). \quad \text{(B2)}$$

The luminosity L_1 is a function of halo mass and is chosen such that

$$\tilde{\Phi}^* \Gamma(\tilde{\alpha}+1, L_1/\tilde{L}^*) = 1; \quad \text{(B3)}$$

when choosing the central galaxy luminosity, we assume that L_c is a random variable drawn from $\Phi(L|M)$ for the range of luminosities $L > L_1$. The remaining $N-1$ galaxies within the halo are assigned luminosities in the range $L_{\rm min} < L < L_1$, drawn at random from the luminosity function (the 'intermediate' approach of Y04).

The penultimate step involves assigning morphological types to each mock galaxy; this is done by defining a function $f_{\rm late}(L, M)$ that specifies the fraction of galaxies with luminosity L in haloes of mass M that are late-type. This function can be expressed as the product of functions

$$f_{\rm late}(L, M) = g(L)h(M)q(L, M), \quad \text{(B4)}$$

where

$$q(L, M) = \begin{cases} 1 & \text{if } g(L)\,h(M) \leq 1 \\ \frac{1}{g(L)\,h(M)} & \text{if } g(L)\,h(M) > 1 \end{cases}, \quad \text{(B5)}$$

$$g(L) = \frac{\hat{\Phi}_{\rm late}(L)}{\hat{\Phi}(L)} \frac{\int_0^\infty \Phi(L|M)\,n(M)\,{\rm d}M}{\int_0^\infty \Phi(L|M)\,h(M)\,n(M)\,{\rm d}M}, \quad \text{(B6)}$$

and

$$h(M) = \max\left(0, \min\left[1, \left(\frac{\log(M/M_a)}{\log(M_b/M_a)}\right)\right]\right). \quad \text{(B7)}$$

Here, $n(M)$ is the halo mass function (Sheth & Tormen 1999), $\hat{\Phi}_{\rm late}(L)$ and $\hat{\Phi}(L)$ correspond to the *observed* luminosity functions of the late-type and entire galaxy samples, respectively, and M_a and M_b are free parameters defined as the masses at which $h(M)$ takes on the values 0 and 1, respectively. van den Bosch et al. (2003) demonstrated that this parametrization allowed the galaxy population to be split into early- and late-types such that the respective luminosity functions and clustering properties could be recovered. We follow Y04 in adopting $M_{\rm a} = 10^{17.26}\,h^{-1}\,{\rm M}_\odot$ and $M_{\rm b} = 10^{10.86}\,h^{-1}\,{\rm M}_\odot$. Formally, we assign morphological type by drawing a random number R that is uniformly distributed between [0, 1] and comparing it to $f_{\rm late}(L, M)$. If $R < f_{\rm late}(L, M)$, the galaxy is designated late-type, otherwise it is early-type.

The final step involves assigning phase-space coordinates (i.e. positions and velocities) to each of the N galaxies within the halo. The brightest central galaxy is associated with the most bound particle of the halo and is assigned its position and velocity. The remaining $N-1$ galaxies can be treated in a variety of ways. For the purposes of this study, in which our main concern is testing the reliability of our selection criteria, we follow Y04 in randomly sampling dark matter particles from the FOF group (their 'FOF approach'). More sophisticated approaches, in which we explicitly track the merging history of individual haloes, will be essential for future work, especially with regard to kinematics (Power et al., in preparation).

APPENDIX C: GALAXY CLASSIFICATION

Our primary classification method is that of Bailin & Harris (2008b), which has been validated using high-quality imaging from the Millennium Galaxy Catalogue (Liske et al. 2003). However, given the qualitative difference between our results for the different subpopulations, it is important to confirm that the difference seen is not an artefact of the galaxy classification scheme. We examine how the anisotropy of the satellite distribution varies using other methods, such as the following.

(i) Inclination-corrected location on the colour–magnitude diagram (CMD$^{\rm F}$), which is strongly bimodal (Bailin & Harris 2008b). Galaxies are considered 'early' if they are redder than CMD$^{\rm F} = -0.05$, and 'late' if they are bluer.

(ii) Spectroscopic principal component analysis (PCA) eClass parameter. Galaxies are considered 'early' if they have eClass < -0.07, otherwise they are considered 'late'.

(iii) The inclination-corrected global concentration of the light profile, $C_{\rm norm}$. The distribution of galaxy concentrations is trimodal (Bailin & Harris 2008a). We label the 'Elliptical' (high-$C_{\rm norm}$ and high-b/a) region from Bailin & Harris (2008a) as 'early', their 'Disc' (low-$C_{\rm norm}$) region as 'late' and all other galaxies as 'intermediate'.

It should be noted that these measurements are completely independent: the CMD location is based on global photometry, the PCA analysis is based on spectroscopy and the concentration is based on the distribution of the light profile.

The results using these alternative classification schemes are shown in Fig. C1. The mean disc angle and KS test probability that each sample is drawn from an isotropic distribution are also given. The major-axis distribution around early-type galaxies and a distribution consistent with isotropy around late-type galaxies are seen using every method. Intermediate-type galaxies are red with intermediate concentrations; the galaxies with red CMD$^{\rm F}$ and with intermediate $C_{\rm norm}$ show the same major-axis distribution as around the intermediate-type galaxies of Bailin & Harris (2008b). Therefore, although the magnitude of the measured anisotropy varies at a $\sim 1\sigma$ level, the detected anisotropy cannot be simply a galaxy classification artefact: satellites of early- and late-type galaxies have different angular distributions.

We note that the classification of some of our galaxies is uncertain. Because the galaxies that constitute our primary sample are typically more luminous and more isolated than typical SDSS spectroscopic galaxies, they provide a biased sample of parameter space. In particular, several of our primary galaxies have $C_{\rm norm} < 1$ (i.e. they have low concentrations) but have CMD$^{\rm F} > -0.05$ (i.e. they are red): 4.3 per cent of all primaries and 12.0 per cent of primaries classified as late-type fall into this region of parameter space, compared to just 1.8 per cent of the visually classified galaxies in Bailin & Harris (2008b) and 3.6 per cent of those classified as late. Given that the anisotropy of the satellite distribution differs between galaxy classes, and shows the strongest difference between the late- and intermediate-types, examining the anisotropy around the galaxies in this region of parameter space can provide insight into their nature.

If we separate our late-types into red and blue sub-classes (divided at CMD$^{\rm F} = -0.05$, as above), we find that the mean disc angle around the blue subclass is $46\overset{\circ}{.}7 \pm 2\overset{\circ}{.}2$, consistent with isotropy and with the results from the full late-type sample. However, the mean disc angle around the red subclass is $37\overset{\circ}{.}3^{+5\overset{\circ}{.}0}_{-5\overset{\circ}{.}5}$, exhibiting major-axis alignment consistent with the results from the intermediate-type sample. This suggests that the red low-concentration galaxies more properly belong to the intermediate classification.

APPENDIX D: ANGULAR DISTRIBUTION OF SATELLITES IN THE MOCK CATALOGUES

To confirm that our measurement of an anisotropic distribution of satellite galaxies is due to an intrinsic anisotropy rather than an

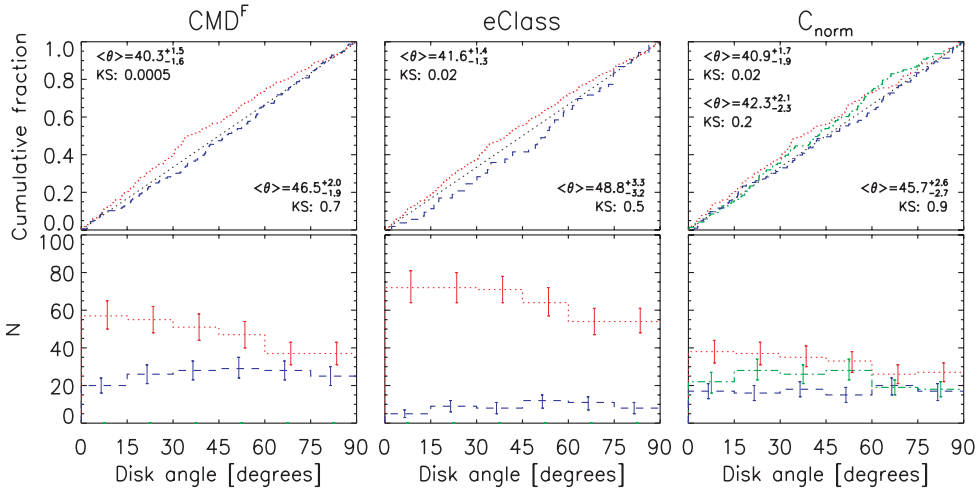

Figure C1. Cumulative (top panels) and differential (bottom panels) distributions of satellite disc angles of primary galaxies classified using the following schemes (left- to right-hand panels): CMD^F, spectroscopic eClass parameter and inclination-corrected Petrosian concentration parameter C_{norm}. Colours/line styles are as in Fig. 4. Mean disc angles and KS test probabilities that the samples are drawn from a uniform distribution are given in the top left-hand corner (bottom right-hand corner) of the cumulative plots for the early-type (late-type) samples. The statistics for the intermediate-type samples are given below the early-type statistics for C_{norm}.

artefact of our method, we have performed an identical analysis on the mock catalogues, whose satellite distributions are, by construction, isotropic. We use mock catalogues generated from the five independent $100\,h^{-1}$ Mpc simulations in order to account for cosmic variance. The distributions are plotted in Fig. D1 and the statistical measures of anisotropy are listed in Table D1.

The level of anisotropy that we measure from isotropically distributed satellites in the mock catalogues is small. Even when the isotropic KS test probabilities in the mock samples are low, the deviations are not systematic: the mean disc angle almost always deviates from 45° by less than 2° and the polar fraction never deviates from 0.5 by more than 4 per cent. These are much smaller than the anisotropies that we detect around early-type galaxies in the observational sample, confirming that our detection of anisotropy cannot be explained by intrinsically isotropically distributed satellites.

APPENDIX E: DETERMINATION OF THE LSS AXIS

The physical environment of a galaxy is best described by the region in which the presence of the galaxy predicts the presence of other matter; the radial extent of this region is characterized by the correlation length r_0. For the global $\sim L^*$ galaxy population, $r_0 \sim 4$–$6\,h^{-1}$ Mpc (Norberg et al. 2002). However, the isolated galaxies that constitute our sample are, by construction, much less clustered than average; for example, H I-selected galaxies, which are much less likely than average to have large nearby neighbours, have a much smaller $r_0 \sim 3.3\,h^{-1}$ Mpc (Basilakos et al. 2007; Meyer et al. 2007). For our very isolated sample, $3\,h^{-1}$ Mpc is a reasonable radius in which to characterize the large-scale environment of each galaxy.

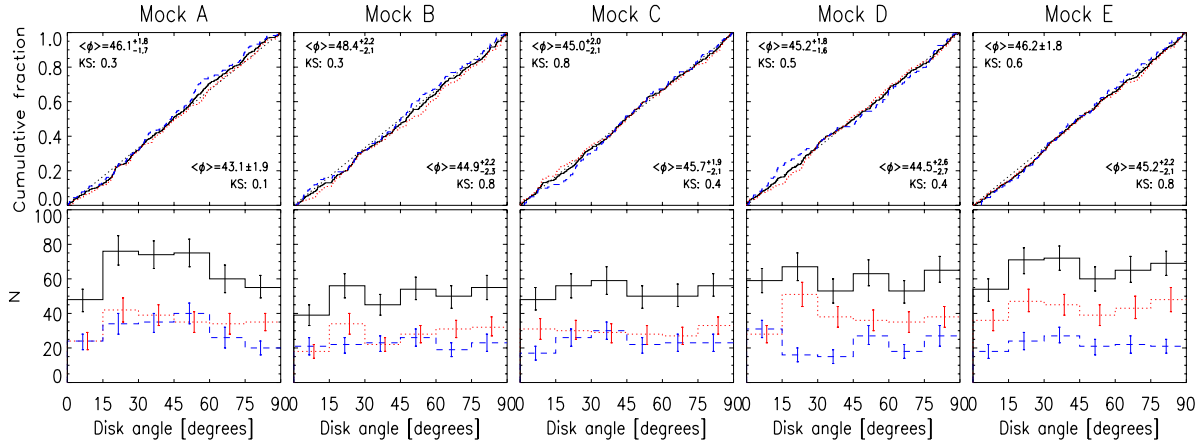

Figure D1. Cumulative (top panels) and differential (bottom panels) distributions of satellite disc angles in the five mock catalogues. Colours/line styles are as in Fig. 4. Mean disc angles and KS test probabilities that the samples are drawn from a uniform distribution are given in the top left-hand corner (bottom right-hand corner) of the cumulative plots for the early-type (late-type) samples.

Table D1. Anisotropy of satellites in mock catalogues.

Parameter	Mock A	Mock B	Mock C	Mock D	Mock E
Full sample					
KS probability	0.28	0.41	0.95	0.94	0.65
Mean disc angle [°]	$44.7^{+1.4}_{-1.2}$	46.8 ± 1.5	45.3 ± 1.5	$44.9^{+1.5}_{-1.4}$	$45.9^{+1.5}_{-1.4}$
Median disc angle [°]	$44.7^{+2.1}_{-2.0}$	$47.4^{+1.7}_{-2.2}$	$44.4^{+2.9}_{-1.7}$	$45.4^{+2.5}_{-2.7}$	$44.1^{+3.0}_{-1.6}$
Polar fraction	0.49 ± 0.03	0.53 ± 0.03	0.49 ± 0.03	0.50 ± 0.03	0.50 ± 0.03
Early-type primaries					
KS probability	0.30	0.33	0.76	0.46	0.64
Mean disc angle [°]	$46.1^{+2.0}_{-1.7}$	48.4 ± 2.2	$45.0^{+2.2}_{-1.9}$	45.2 ± 1.7	$46.2^{+1.8}_{-1.7}$
Median disc angle [°]	$44.9^{+4.2}_{-1.9}$	$48.8^{+5.8}_{-1.4}$	$44.8^{+3.2}_{-2.1}$	$44.0^{+3.4}_{-1.8}$	$45.2^{+1.9}_{-3.5}$
Polar fraction	$0.50^{+0.03}_{-0.04}$	0.55 ± 0.04	0.49 ± 0.04	0.48 ± 0.03	0.50 ± 0.03
Late-type primaries					
KS probability	0.10	0.83	0.45	0.40	0.80
Mean disc angle [°]	$43.1^{+2.0}_{-1.8}$	$44.9^{+2.3}_{-2.2}$	$45.7^{+2.0}_{-2.2}$	$44.5^{+2.6}_{-2.4}$	45.2 ± 2.2
Median disc angle [°]	$43.7^{+2.4}_{-2.7}$	$45.2^{+2.9}_{-2.2}$	$43.7^{+4.1}_{-3.2}$	$47.9^{+5.1}_{-9.4}$	$43.4^{+6.6}_{-4.0}$
Polar fraction	0.48 ± 0.04	0.51 ± 0.04	$0.48^{+0.5}_{-0.4}$	0.54 ± 0.05	0.48 ± 0.05

We therefore determine the PA of the LSS around each primary galaxy by diagonalizing the moment of inertia tensor of the projected positions of all spectroscopic galaxies with projected radii of between 1000 and 3000 h^{-1} kpc (thereby explicitly ensuring that there is no overlap between the galaxies used to determine the orientation of the LSS and those used to evaluate the isolation of the primary or the satellites themselves) and with velocities that differ from that of the primary by no more than 400 km s^{-1} (this is larger than the 300 km s^{-1} Hubble flow component in order to account for the peculiar velocities of galaxies, which have a dispersion of 85 km s^{-1} in the local volume; Karachentsev et al. 2003).

We have used the mock catalogues to confirm that this procedure reliably recovers the three-dimensional PA of the LSS surrounding the primary. We have taken the known three-dimensional positions of all haloes within a spherical volume of 3000 h^{-1} kpc around the halo of each primary galaxy in the mock catalogues, constructed and diagonalized their inertia tensor and projected the major axis on to the plane of the sky. The PA of this axis is then compared to the two-dimensional PA inferred from the 'observed' galaxies in the mock catalogues. The cumulative distribution of the misalignment between the PA determined using three-dimensional positions and that inferred from the two-dimensional observables is plotted in Fig. E1. To improve the statistics, we have included in this plot all galaxies that match the isolation criteria, regardless of whether they have satellites; however, the results are consistent if we restrict the sample to just those with satellites. The solid line indicates the relative alignment when both the three-dimensional LSS PA and the inferred two-dimensional are well-defined (i.e. that contain galaxies within the defining sphere or cylinder), and has a median misalignment of 13°.8. A small fraction of galaxies have well-defined two-dimensional LSS PAs, and would therefore be included in the observational analysis, but no well-defined three-dimensional LSS axis because none of the galaxies that lies within the redshift-space cylinder lies within the three-dimensional sphere. We account for these cases by assuming that their intrinsic three-dimensional LSS PAs are isotropically distributed and indicate the alignment of the full sample including them as the dashed line in Fig. E1. Half of the LSS PAs are aligned to within 15°.8, therefore, this procedure successfully recovers the PA of the LSS.

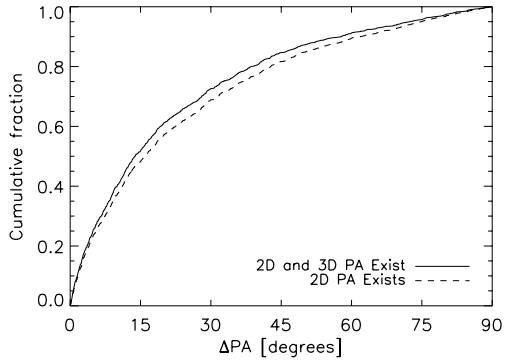

Figure E1. Cumulative distribution of the difference between the PA of the LSS measured around isolated mock galaxies using the 'observed' two-dimensional galaxy positions and redshifts versus that measured using the known three-dimensional positions of surrounding haloes. The solid line indicates galaxies for which both the two- and three-dimensional PA is well-defined, while the dashed line also includes haloes for which only the two-dimensional PA is well-defined.

APPENDIX F: COMPARISONS USING DIFFERENT SELECTION CRITERIA

In Fig. 14, we have compared the mean disc angle determined by previous studies of satellite anisotropy to the values we derive using identical selection criteria.

No previous study has identified intermediate-type galaxies as a separate class; we therefore adopt a simple binary classification based on the location of the galaxy on the CMD: a galaxy is considered early-type if its $^{0.1}(g-r)$ colour is redder than

$$^{0.1}(g-r) = 0.70 - 0.0325(M_r - 5\log h + 19) \quad \text{(F1)}$$

and late-type if it is bluer than this threshold. The results of Appendix C indicate that different methods of classifying galaxies may introduce $\sim 1\sigma$ differences in the measured anisotropy.

We split each sample by the galaxy type of its primary although ZSFW and B05 only studied late-types, and B05 did not separate the sample by type. B05 suggested that her samples were dominated by systems with late-type primaries; in contrast, we find

that 46/58/37 per cent of the primaries we select using her criteria are classified as early-types according to Bailin & Harris (2008b), containing 52/64/43 per cent of the satellites for samples 1, 2, and 3, respectively. Using the location on the CMD, the fraction of early-type primaries is even higher: 85/90/83 per cent containing 89/94/86 per cent of the satellites.

SL04 do not quote a mean disc angle. Rather they fit the distribution of disc angles θ to the form

$$f(\theta) = A\cos(2\theta) + B \tag{F2}$$

and quote the values of A and errors σ_A. To enable a more direct comparison with other studies, we calculate the mean disc angle of the associated distribution as

$$\langle\theta\rangle = \frac{\pi}{4} - \frac{A}{2} \tag{F3}$$

with uncertainty

$$\sigma_{\langle\theta\rangle} = \frac{\sigma_A}{2}, \tag{F4}$$

in radians. APPZ also do not quote a mean disc angle. We have derived the mean and the error of the distributions from their plotted histograms, assuming that all satellites lie at the central value of the bin they fall in. The errors are calculated by bootstrap resampling. ZSFW do not quote a mean disc angle, but it can be derived from the data in table 2 of Zaritsky et al. (1997a). The errors are calculated by bootstrap resampling.

The only cases where our results deviate from the previous results by more than 2σ are the early-type samples of APPZ. Even in these cases, the sense of the observed anisotropy is the same, only the magnitude is different. These are cases where there is no mean disc angle quoted by the authors, and therefore we have used indirect methods to determine the appropriate mean; they also use different methods to classify early-type galaxies. We conclude that the numerical differences in these cases are not significant.

SUPPORTING INFORMATION

Additional Supporting Information may be found in the online version of this article:

Table 4. Data for primary and satellite galaxies.

Please note: Wiley-Blackwell is not responsible for the content or functionality of any supporting information supplied by the authors. Any queries (other than missing material) should be directed to the corresponding author for the article.

This paper has been typeset from a TEX/LATEX file prepared by the author.